Kondo physics in double quantum dot based Cooper pair splitters

Kacper Wrześniewski and Ireneusz Weymann*
Faculty of Physics, Adam Mickiewicz University, ul. Umultowska 85, 61-614 Poznań, Poland
(Received 21 August 2017; revised manuscript received 23 October 2017; published 6 November 2017)

The Andreev transport properties of double quantum dot based Cooper pair splitters with one superconducting and two normal leads are studied theoretically in the Kondo regime. The influence of the superconducting pairing correlations on the local density of states, Andreev transmission coefficient, and Cooper pair splitting efficiency is thoroughly analyzed. It is shown that finite superconducting pairing potential quickly suppresses the SU(2) Kondo effect, which can however reemerge for relatively large values of coupling to superconductor. In the SU(4) Kondo regime, a crossover from the SU(4) to the SU(2) Kondo state is found as the coupling to superconductor is enhanced. The analysis is performed by means of the density-matrix numerical renormalization group method.

DOI: 10.1103/PhysRevB.96.195409

I. INTRODUCTION

Creation, manipulation, and detection of entangled pairs of electrons is an important requirement for engineering quantum information and computation protocols in solid state systems [1–3]. As a natural source of entangled electrons one can consider superconductors, in which two electrons with opposite spins form spin singlet states—the Cooper pairs [4–6]. It has been demonstrated experimentally that it is possible to extract and split Cooper pairs in a double quantum dot (DQD) setup involving one superconductor (SC) and two normal (N) leads, each attached to a different quantum dot [7–14]. In such a Cooper pair splitter (CPS), when the bias voltage eV applied between the SC and N leads is smaller than the superconducting energy gap Δ, the current flows through the system due to the Andreev reflection processes [15]. One can generally distinguish two types of such processes: (i) direct Andreev reflection (DAR), in which the Cooper pair electrons tunnel through one arm of the device, and (ii) crossed Andreev reflection (CAR), when the Cooper pair electrons become split and each electron leaves the superconductor through a different arm of the device [16,17]. Since the latter processes are crucial for the creation of entangled electrons, it is important to optimize the splitting efficiency η of the device, i.e., to enhance the rate of CAR processes as compared to the DAR processes. This can be obtained, for example, by tuning the position of the DQD's energy levels and setting the system in an appropriate transport regime [7,10].

Transport properties of double quantum dots with superconducting contacts have been recently explored both experimentally [7–14,18] and theoretically [19–27]. The theoretical investigations were however mostly devoted to transport properties in a relatively weak coupling regime. Various geometries of the system were considered, with the two dots attached to the leads forming either serial [19], T-shaped [22], or CPS fork configurations [24,25]. In particular, the emergence of the triplet blockade and its influence on transport were analyzed, as well as various Andreev bound states (ABS) splitting mechanisms [20,25]. Moreover, unconventional pairing [24] in the presence of inhomogeneous magnetic field was predicted and the role of the spin-orbit interaction on nonlocal entanglement was demonstrated [26]. Other important aspects of transport in such systems, such as the current and noise correlations [21,27] and spin dependence of transport controlled by means of ferromagnetic contacts [23,25,27], were also thoroughly discussed.

In this paper we extend those studies by focusing on the Andreev transport in the strong coupling regime, where electronic correlations can give rise to the Kondo effect [28,29]. When a spin one-half impurity is coupled to the conduction band of a metallic host, for temperatures T lower than the Kondo temperature T_K, the conduction electrons screen the impurity's spin and a delocalized singlet state is formed. Its emergence results in the formation of an additional peak at the Fermi energy in the local density of states [29]. For single quantum dots, in the case of spin SU(2) Kondo effect, this leads to an enhancement of the conductance to its maximum value of $2e^2/h$ [30,31]. For double quantum dots, depending on the DQD occupation, one can observe different types of the Kondo effect. In particular, when both the spin and orbital degrees of freedom are degenerate, an SU(4) Kondo state is formed in the system [32,33].

When the leads are superconducting the situation becomes much more interesting [34–38]. First of all, for dot coupled to superconductor, the occurrence of the Kondo phenomenon is conditioned by the ratio of the Kondo temperature to the superconducting energy gap T_K/Δ, and a quantum phase transition occurs as this ratio is varied [35,39–42]. Furthermore, for two-terminal hybrid junctions involving quantum dot and N and SC leads, the Kondo state can be formed by screening the dot's spin by the normal lead [34,35], while finite coupling to SC lead can result in an enhancement of the Kondo temperature [43].

From the theoretical side, the accurate studies of transport properties of nanostructures in nonperturbative regime require resorting to sophisticated numerical methods. One of them is the density-matrix numerical renormalization group (DM-NRG) method [44,45], which allows for obtaining results of very high accuracy on the transport behavior of the considered system [46]. In these considerations we employ DM-NRG to address the problem of the Kondo effect and Andreev transport in double quantum dot based Cooper pair splitters. In particular, we study the DQD energy level dependence of the local density of states as well as the Andreev transmission coefficient, together with the splitting efficiency of the device. We then focus on the two transport regimes when the system in the absence of coupling to superconductor exhibits either the SU(2) or the SU(4) Kondo effect, and study the influence

*weymann@amu.edu.pl

of superconducting pairing correlations on these two types of Kondo state. We show that, contrary to single quantum dots [43,47], the SU(2) Kondo state becomes quickly suppressed by even small superconducting pairing potential. On the other hand, the pairing correlations result in a crossover from the SU(4) to the SU(2) Kondo effect.

The paper is organized as follows. In Sec. II we present the model, Hamiltonian, and method used in calculations, and describe the main quantities of interest. Section III is devoted to numerical results and their discussion. In Secs. III A and III B we analyze the DQD level dependence of the local density of states and the Andreev transmission coefficient, together with splitting efficiency, respectively. The SU(2) [SU(4)] Kondo regime is thoroughly discussed in Sec. III C (Sec. III D). Finally, the conclusions can be found in Sec. IV.

II. THEORETICAL DESCRIPTION

A. Model and parameters

The considered system consists of two single level quantum dots attached to an s-wave superconductor (SC) and coupled to two normal (N) electrodes; see Fig. 1. The Hamiltonian of isolated double quantum dot has the form

$$H_{DQD} = \sum_{j\sigma} \varepsilon_j d^\dagger_{j\sigma} d_{j\sigma} + \sum_j U_j n_{j\uparrow} n_{j\downarrow} + \sum_{\sigma\sigma'} U_{LR} n_{L\sigma} n_{R\sigma'}, \tag{1}$$

with $d^\dagger_{j\sigma}$ creating a spin-σ electron in dot j of energy ε_j. The on-dot Coulomb correlations are denoted by U_j, with $n_{j\sigma} = d^\dagger_{j\sigma} d_{j\sigma}$, while the interdot Coulomb interactions are described by U_{LR}. The normal electrodes are modeled as free quasiparticles by the Hamiltonian, $H_N = \sum_{j\mathbf{k}\sigma} \varepsilon_{j\mathbf{k}} c^\dagger_{j\mathbf{k}\sigma} c_{j\mathbf{k}\sigma}$, where $c^\dagger_{j\mathbf{k}\sigma}$ is the creation operator for an electron with spin σ, wave number $\mathbf{k}$, and energy $\varepsilon_{j\mathbf{k}}$ in the jth lead. The BCS superconductor is modeled by $H_S = \sum_{\mathbf{k}\sigma} \xi_{\mathbf{k}} a^\dagger_{\mathbf{k}\sigma} a_{\mathbf{k}\sigma} + \Delta \sum_{\mathbf{k}} (a_{\mathbf{k}\downarrow} a_{-\mathbf{k}\uparrow} + \text{H.c.})$, where $a^\dagger_{\mathbf{k}\sigma}$ creates an electron with momentum $\mathbf{k}$, spin σ, and energy $\xi_{\mathbf{k}}$. The superconducting order parameter, assumed to be real, is denoted by Δ. The double dot is coupled to external leads by the tunneling Hamiltonian

$$H_T = \sum_{j\mathbf{k}\sigma} \left(V_{j\mathbf{k}} c^\dagger_{j\mathbf{k}\sigma} d_{j\sigma} + V^S_{j\mathbf{k}} a^\dagger_{\mathbf{k}\sigma} d_{j\sigma} + \text{H.c.} \right), \tag{2}$$

where the tunnel matrix elements between the dot j and the normal lead j (superconductor) are denoted by $V_{j\mathbf{k}}$ ($V^S_{j\mathbf{k}}$). Assuming momentum independent tunnel matrix elements, the coupling between the dot j and the corresponding normal electrode is described by $\Gamma_j = \pi |V_j|^2 \rho_j$, where ρ_j is the density of states of lead j. On the other hand, the coupling between the dot j and superconductor is given by $\Gamma^S_j = \pi |V^S_j|^2 \rho_S$, with ρ_S the density of states of the superconductor in the normal state.

In our considerations we focus on the Andreev transport regime; therefore, to exclude the normal tunneling processes, in the following we take the limit of infinite superconducting energy gap. In this limit the double dot coupled to superconductor can be described by the effective Hamiltonian of the form [20,25,48]

$$H^{\text{eff}}_{DQD} = H_{DQD} - \sum_j \Gamma^S_j (d^\dagger_{j\uparrow} d^\dagger_{j\downarrow} + d_{j\downarrow} d_{j\uparrow}) + \Gamma^S_{LR} (d^\dagger_{L\uparrow} d^\dagger_{R\downarrow} + d^\dagger_{R\uparrow} d^\dagger_{L\downarrow} + d_{R\downarrow} d_{L\uparrow} + d_{L\downarrow} d_{R\uparrow}). \tag{3}$$

Now, the proximity effect is included through pairing potential induced in the DQD, where the first term, proportional to Γ^S_j, describes the direct Andreev reflection (DAR) processes, while the last term, proportional to $\Gamma^S_{LR} = \sqrt{\Gamma^S_L \Gamma^S_R}$, corresponds to the crossed Andreev reflection (CAR) processes. In DAR processes Cooper pairs are transferred through one arm of the splitter. On the other hand, in CAR processes Cooper pair electrons become split and each electron leaves the superconductor through a different junction with normal lead.

The effective double dot Hamiltonian is not diagonal in the local basis defined by the states $|\chi_L \chi_R\rangle = |\chi_L\rangle |\chi_R\rangle$, in which the left (right) dot is in state $|\chi_L\rangle$ ($|\chi_R\rangle$), with $\chi_j = 0, \sigma, d$, for empty, singly occupied, and doubly occupied dot j. Because the effective Hamiltonian commutes with the total spin operator, H^{eff}_{DQD} has a block-diagonal form in the corresponding spin quantum number. As we show in the Appendix, the spin triplet space is quite trivial because it is not affected by the superconducting correlations due to symmetry reasons. In the spin doublet subspace we present a general solution to the eigenproblem. However, in the singlet subspace it is in general not possible to find simple analytical formulas for the eigenstates and eigenenergies; therefore, in this subspace we discuss the eigenspectrum only in some limiting situations. The first one is the particle-hole symmetry point of the model, $\varepsilon = -U/2 - U_{LR}$, and the second one is the fully symmetric SU(4) Kondo regime, $\varepsilon = -U_{LR}/2$ with $U_{LR} = U$. The analytical formulas presented in the Appendix will be crucial to understanding the complex behavior of the system in the considered transport regimes. Moreover, the eigenenergies will help to relate the position of peaks observed in transport quantities to energies of Andreev bound states (ABS), which can be inferred from excitation energies between the corresponding molecular states of the double quantum dot proximized by SC lead.

In our analysis we assume that the system is symmetric, i.e., we set $\Gamma_L = \Gamma_R \equiv \Gamma$ and $\Gamma^S_L = \Gamma^S_R \equiv \Gamma_S$. For the two

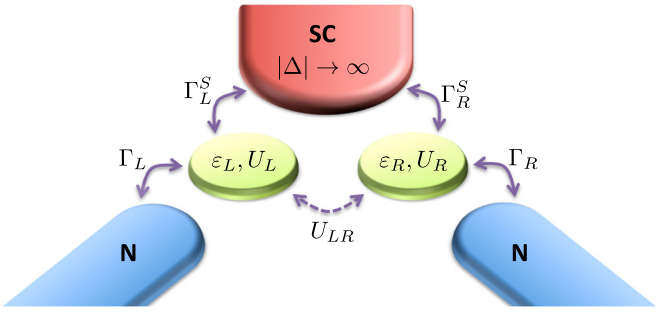

FIG. 1. Schematic of the considered system. Two single-level quantum dots, described by on-site energy ε_j ($j = L$ for left and $j = R$ for right dot) and Coulomb correlations U_j are coupled to a common s-wave superconductor (SC), with coupling strength Γ^S_j, and attached to two separate normal (N) electrodes, with coupling strength Γ_j. The two dots are coupled capacitively by U_{LR}.

quantum dots we also assume $U_L = U_R \equiv U$ and $\varepsilon_L = \varepsilon_R \equiv \varepsilon$. To perform the calculations, we set $U \equiv 1$ and take $U_{LR} = U/2$ and $\Gamma = U/20$. We note that since both the couplings and the position of the DQD levels can be tuned individually by applied gate voltages [33], the chosen set of parameter is of relevance for current and future experiments. We also notice that a weak left-right asymmetry would induce rather quantitative changes to the results we present and discuss in the following, while qualitatively we expect our predictions to be relevant. However, the assumption of the superconducting energy gap being the largest energy scale in the problem needs to be treated with a certain care. While this assumption allows us to focus exclusively on the behavior of Andreev reflection processes, and for that reason it was adapted in many previous theoretical works [19,20,24,25,49–59], from an experimental point of view, the condition $\Delta > U$ does not need to be fulfilled in any Cooper pair splitting device. Nevertheless, there are superconductors, in which the gap is of the order of a couple of meV [60]; consequently, experimental realizations of splitters with large Δ should be possible.

B. Quantities of interest and method

The main quantity of interest is the transmission coefficient for Andreev reflection processes, $T_A(\omega)$, which can be written as

$$T_A(\omega) = T_A^{\mathrm{DAR}}(\omega) + T_A^{\mathrm{CAR}}(\omega), \tag{4}$$

where the first term describes the transmission due to DAR processes, which is explicitly given by

$$T_A^{\mathrm{DAR}}(\omega) = 4\sum_{j\sigma}\Gamma_j^2 \left|\langle\langle d_{j\sigma}|d_{j\bar{\sigma}}\rangle\rangle_\omega^r\right|^2, \tag{5}$$

while the last term denotes the transmission coefficient due to CAR processes and is described by

$$T_A^{\mathrm{CAR}}(\omega) = 4\Gamma_L\Gamma_R\sum_{\sigma}\left[|\langle\langle d_{L\sigma}|d_{R\bar{\sigma}}\rangle\rangle_\omega^r|^2 + |\langle\langle d_{R\sigma}|d_{L\bar{\sigma}}\rangle\rangle_\omega^r|^2\right]. \tag{6}$$

Here, $\langle\langle A|B\rangle\rangle_\omega^r$ is the Fourier transform of the retarded Green's function, $\langle\langle A|B\rangle\rangle_t^r = -i\Theta(t)\langle\{A(t), B(0)\}\rangle$. The DAR and CAR transmission coefficients can be used to define the Cooper pair splitting efficiency of the device as

$$\eta = \frac{T_A^{\mathrm{CAR}}(\omega)}{T_A^{\mathrm{CAR}}(\omega) + T_A^{\mathrm{DAR}}(\omega)}. \tag{7}$$

When $\eta \to 1$, transport is exclusively due to CAR processes, which means that each Cooper pair leaving the superconductor becomes split into two separate leads. On the other hand, if only DAR processes are responsible for Andreev transport, $\eta \to 0$.

With the Andreev transmission coefficient, it is possible to determine the Andreev current flowing between the superconductor and the normal leads [23]

$$I_A(V) = \frac{e}{h}\int d\omega[f(\omega - eV) - f(\omega + eV)]T_A(\omega), \tag{8}$$

where $f(\omega)$ denotes the Fermi-Dirac distribution function and it is assumed that the chemical potential of the left and right lead is equal to eV, while the superconductor is grounded. From the above formula it is easy to find the Andreev differential conductance, which in the limit of vanishing temperature can be approximated by

$$G_A(V) \approx \frac{e^2}{h}[T_A(\omega = eV) + T_A(\omega = -eV)]. \tag{9}$$

Consequently, the measurement of differential conductance allows one to probe the energy dependence of the Andreev transmission coefficient.

Another interesting quantity is the local density of states, which is given by the total normalized spectral function

$$\mathcal{A} = \sum_{ij}\mathcal{A}_{ij} = -\sum_{ij}\sqrt{\Gamma_i\Gamma_j}\,\mathrm{Im}\langle\langle d_{i\sigma}|d_{j\sigma}^\dagger\rangle\rangle_\omega^r. \tag{10}$$

Thus $\mathcal{A}_i \equiv \mathcal{A}_{ii}$ corresponds to the local density of states of one of the quantum dots, while $\mathcal{A}_{ij}$ describes the cross correlations between the two quantum dots generated by proximity-induced interdot pairing potential Γ_{LR}^S. Because we consider a symmetric situation, $\mathcal{A}_L = \mathcal{A}_R$, and $\mathcal{A}_{LR} = \mathcal{A}_{RL}$.

To determine the relevant correlation functions we use the density-matrix numerical renormalization group method [44–46]. This nonperturbative method allows for obtaining very accurate results on the static and dynamic properties of the system. In NRG, the initial Hamiltonian is transformed to an NRG Hamiltonian, in which the leads are modeled as tight-binding chains with appropriate hopping integrals [44]. The calculations are performed in an iterative fashion by keeping an assumed number N_K of the lowest-energy eigenstates. Here, we exploited the full spin symmetry of the system and kept at least $N_K = 2000$ states per iteration. The imaginary parts of the Green's functions were determined from discrete NRG data by performing appropriate broadening [61] and averaging over $N_z = 2$ shifted discretization meshes [62]. The real parts of the Green's functions were obtained from the Kramers-Kronig relation.

C. Stability diagram and transport regimes

The linear Andreev conductance plotted as a function of the position of each dot level assuming a weak coupling between the double dot and normal leads is shown in Fig. 2. The numbers in brackets indicate approximate expectation values of the occupation number of each dot, $(\langle n_L\rangle, \langle n_R\rangle)$, with $n_j = \sum_\sigma n_{j\sigma}$. The conductance was calculated using the rate equations within the sequential tunneling approximation [25]. We note that although this method is not suitable for capturing the correlation effects studied here, it allows us to indicate the considered transport regimes in the phase diagram of the device. In this paper we in particular focus on the symmetric case, $\varepsilon_L = \varepsilon_R \equiv \varepsilon$, a cross section of Fig. 2 marked with a dashed line. By sweeping ε, which can be experimentally done with gate voltages [33], the device can be tuned from the empty or fully occupied orbital regime to the SU(4) and SU(2) Kondo regimes, respectively.[1] The SU(4)

[1]Note that the SU(2) and SU(4) Kondo regimes can be greatly modified by finite coupling to superconductor, such that the Kondo effect can even become fully suppressed. Therefore, referring to the appropriate Kondo regime should be considered as a guide to estimate the corresponding parameter space in the phase diagram of the device in the limit of weak coupling to superconductor.

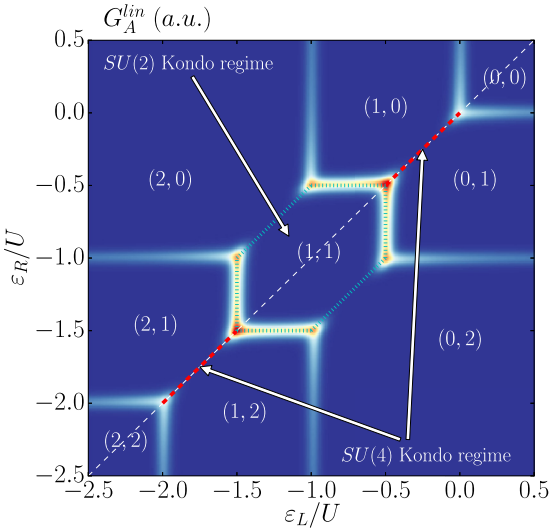

FIG. 2. Linear Andreev conductance $G_A^{\rm lin}$ calculated as a function of the position of each dot level, ε_L and ε_R, using the rate equations. The parameters are $U = 1$, $U_{LR} = U/2$, $\Gamma = U/100$, and $\Gamma_S = U/10$. The numbers in brackets indicate the average occupation of each dot, $(\langle n_L\rangle, \langle n_R\rangle)$, with $n_j = \sum_\sigma n_{j\sigma}$.

Kondo regime is marked with a thick dashed line, while the SU(2) Kondo regime is surrounded by dotted lines in Fig. 2. These transport regimes will be studied in detail in the next sections, and the influence of the proximity-induced pairing potential on the corresponding Kondo states will be thoroughly analyzed.

III. RESULTS AND DISCUSSION

In this section we present and discuss the main results on the local density of states and the Andreev transmission coefficient. We will first study the general gate voltage dependence of transport characteristics assuming $\varepsilon_L = \varepsilon_R \equiv \varepsilon$, i.e., along the dashed line marked in Fig. 2. Then, we shall focus on some more relevant transport regions, including the SU(2) and SU(4) Kondo regimes.

A. Local density of states

The normalized spectral function plotted as a function of energy ω and DQD level position $\varepsilon_L = \varepsilon_R \equiv \varepsilon$ is shown in Fig. 3. This figure is calculated for different values of the coupling to superconductor, as indicated, and it demonstrates the evolution of local density of states with increasing Γ_S. When $\Gamma_S = 0$, one observes the transport behavior typical for a double quantum dot system [63]; see Fig. 3(a). When the position of the DQD energy levels is lowered, the DQD becomes consecutively occupied with electrons. For $\varepsilon \gtrsim 0$ ($\varepsilon \lesssim -U - 2U_{LR}$), the DQD is empty (fully occupied). When $-U_{LR} \lesssim \varepsilon \lesssim 0$ ($-U - 2U_{LR} \lesssim \varepsilon \lesssim -U - U_{LR}$), the double dot is singly occupied (occupied with three electrons), while for $-U - U_{LR} \lesssim \varepsilon \lesssim -U_{LR}$, the DQD is occupied by two electrons, each located on a different quantum dot. The above energies also specify when the charge on the DQD

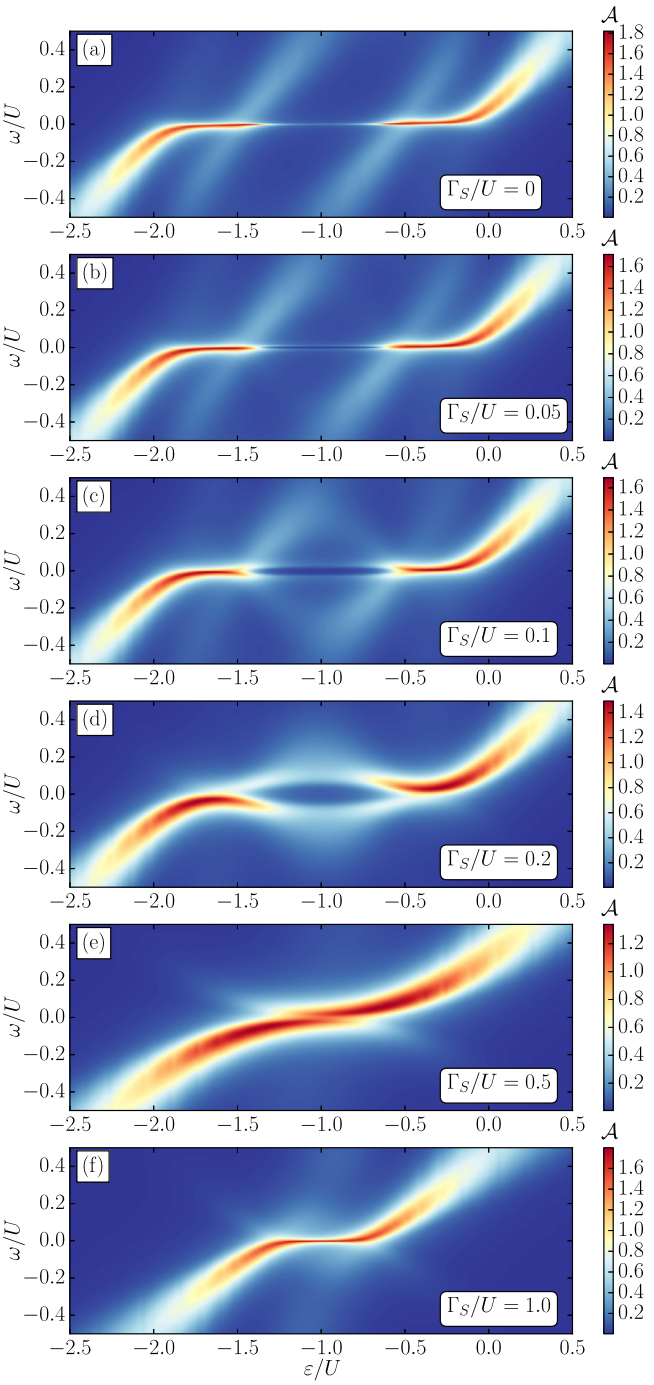

FIG. 3. Total normalized spectral function $\mathcal{A}$ of DQD-based Cooper pair splitter plotted as a function of energy ω and double dot level position, $\varepsilon_L = \varepsilon_R \equiv \varepsilon$, calculated for different values of coupling to superconductor Γ_S, as indicated. The parameters are $U = 1$, $U_{LR} = U/2$, $\Gamma = U/20$, and $T = 0$.

changes and the local density of states exhibits a resonance. In between those resonant energies, the system's spectral function exhibits an enhancement due to the Kondo effect. In the odd occupation regime, i.e., when DQD hosts either one or three electrons, the system exhibits the SU(4) Kondo effect resulting from orbital and spin degeneracies [32,33].

One can estimate the SU(4) Kondo temperature, $T_K^{SU(4)}$, from the half width at half maximum (HWHM) of the Kondo peak in the total spectral function for $\varepsilon = -U_{LR}/2$, which for assumed parameters yields $T_K^{SU(4)}/U \approx 0.017$. On the other hand, when the DQD is occupied by two electrons, each dot exhibits the spin SU(2) Kondo resonance [29,30]. The corresponding Kondo temperature, $T_K^{SU(2)}$, estimated from HWHM of the Kondo resonance in the spectral function for $\varepsilon = -U/2 - U_{LR}$, is equal to $T_K^{SU(2)}/U \approx 10^{-4}$. Note that for the parameters assumed in calculations $T_K^{SU(2)} \ll T_K^{SU(4)}$. This is why in Fig. 3(a) the SU(2) Kondo peak is much less pronounced as compared to the SU(4) Kondo resonance.

When the coupling to superconductor becomes finite, the behavior of the spectral function starts changing. First, one observes the suppression and splitting of the Kondo resonance in the doubly occupied transport regime; see Figs. 3(b)–3(d). This splitting increases with Γ_S; however, when $\Gamma_S \gtrsim U/2$, a single resonance starts forming; see Figs. 3(e) and 3(f). This resonance is again due to the Kondo effect, since for $\Gamma_S \gtrsim U/2$, the doublet state becomes the ground state of the system. On the other hand, the SU(4) Kondo resonance looks much less affected, at least for small values of coupling to superconductor. This is, however, not entirely true, since with increasing Γ_S, the SU(4) Kondo resonance merges with resonance resulting from the formation of Andreev bound states. A thorough discussion of the influence of strength of coupling to superconductor on the corresponding Kondo resonances will be presented in the next sections.

Let us now analyze the behavior of separate contributions, $\mathcal{A}_L$ and $\mathcal{A}_{LR}$, to the total spectral function $\mathcal{A}$. Their energy and DQD energy level dependence is shown in Fig. 4 for $\Gamma_S = U/10$. At first sight, one can notice that the qualitative behavior of $\mathcal{A}$ is mainly determined by the spectral function of single quantum dot $\mathcal{A}_L$. For the considered value of Γ_S, $\mathcal{A}_L$ exhibits a pronounced split Kondo resonance for $-U - U_{LR} \lesssim \varepsilon \lesssim -U_{LR}$ and the SU(4) Kondo resonance when $-U_{LR} \lesssim \varepsilon \lesssim 0$ ($-U - 2U_{LR} \lesssim \varepsilon \lesssim -U - U_{LR}$), similar to the total spectral function; cf. Figs. 4(a) and 4(b).

On the other hand, the off-diagonal spectral function, which accounts for the cross correlations between transport processes through the two dots, behaves in a clearly different manner. First of all, we note that finite value of $\mathcal{A}_{LR}$ results solely from proximity-induced interdot pairing, and it vanishes if CAR processes are not allowed in the system. One can see that $\mathcal{A}_{LR}$ takes considerable values for energies corresponding to resonances in $\mathcal{A}$; cf. Figs. 4(a) and 4(c). Moreover, if on one side of the resonance $\mathcal{A}_{LR}$ is positive, on the other side it changes sign. This effect is most pronounced for $-U_{LR} \lesssim \varepsilon \lesssim 0$ ($-U - 2U_{LR} \lesssim \varepsilon \lesssim -U - U_{LR}$), i.e., when DQD hosts an odd number of electrons; see Fig. 4(c). Positive sign of $\mathcal{A}_{LR}$ can be associated with processes that occur in the same direction through both normal junctions, while negative sign of $\mathcal{A}_{LR}$ indicates that the two processes are anticorrelated [27].

B. Andreev transmission and splitting efficiency

The energy and DQD level dependence of the Andreev transmission coefficient calculated for different values of coupling to superconductor is presented in Fig. 5. When the coupling Γ_S is relatively small, one can see that $T_A(\omega)$ becomes finite in the low-energy regime and it is considerably enhanced for $\varepsilon \approx -U_{LR}$ and $\varepsilon \approx -U - U_{LR}$; see Fig. 5(a). The area when the maximum occurs grows with increasing Γ_S and, at the same time, the maximum value slightly decreases. Moreover, for $\Gamma_S = U/5$, $T_A(\omega)$ becomes finite in almost the whole energy range considered in the figure, with maximum values occurring still for $\varepsilon \approx -U_{LR}$ and $\varepsilon \approx -U - U_{LR}$; see Fig. 5(c). Note that $T_A(\omega)$ exhibits a similar split structure as that visible in the local density of states; cf. Figs. 3(d) and 5(c). Further increase of the coupling strength results in a decrease of the size of the Coulomb blockade regime, which is seen as merging of the two maxima at the particle-hole symmetry point $\varepsilon = -U/2 - U_{LR}$ [Fig. 5(d)]. For even larger Γ_S the transmission coefficient drops and the energy range where $T_A(\omega)$ is enhanced shrinks; see Fig. 5(e).

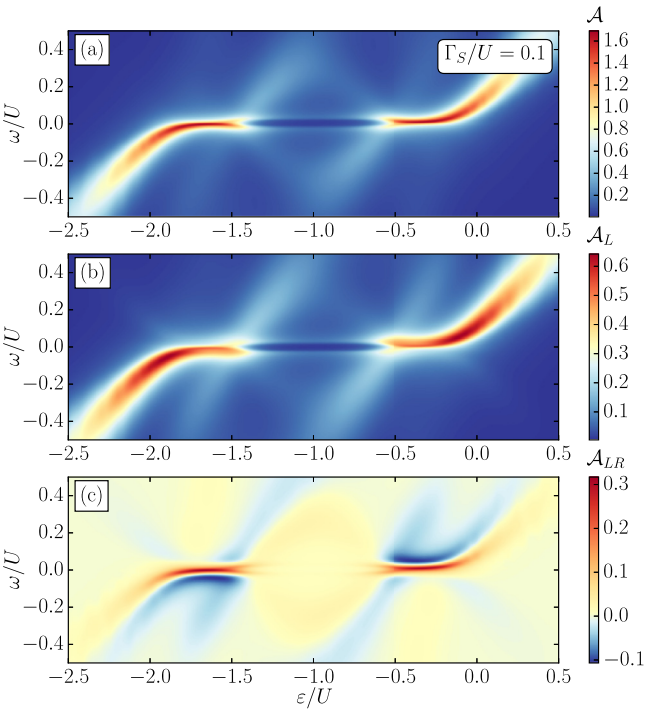

FIG. 4. Normalized spectral function: (a) $\mathcal{A}$, (b) $\mathcal{A}_L$, and (c) $\mathcal{A}_{LR}$, plotted versus energy ω and double dot energy level position ε. The parameters are the same as in Fig. 3 with $\Gamma_S = U/10$.

The different contributions to the transmission coefficient coming from DAR and CAR processes are presented in Fig. 6 for $\Gamma_S = U/10$. The first general observation is that the total Andreev transmission is mainly determined by crossed Andreev reflection processes. This can be expected because the rate of direct Andreev reflection is conditioned by the value of on-site Coulomb correlations, while the rate of CAR processes depends on the interdot correlations. Because $U_{LR} < U$, as in typical experimental realizations [7], one finds more CAR processes compared to DAR ones. This is in fact a very desired situation for Cooper pair splitting experiments, in which one would like to suppress DAR processes and maximize CAR ones.

From the application point of view, it is thus interesting to analyze the Cooper pair splitting efficiency η of the device.

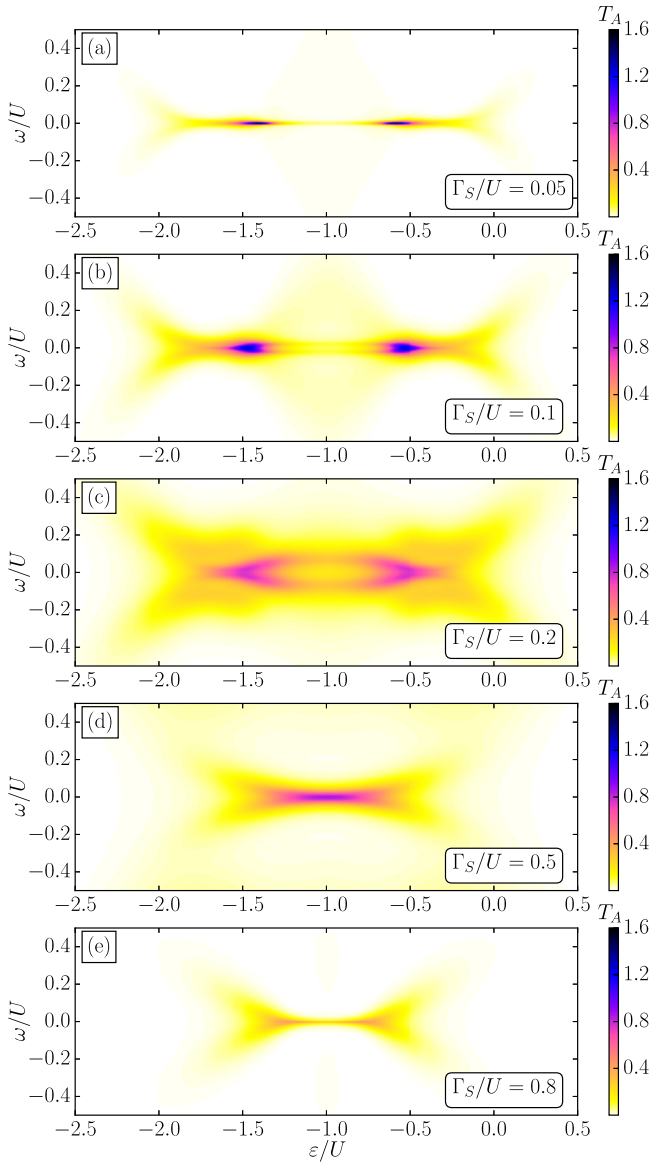

FIG. 5. Andreev transmission coefficient plotted versus energy ω and double dot energy level position ε, and calculated for different values of Γ_S, as indicated. The other parameters are the same as in Fig. 3.

This is presented in Fig. 6(d). One can see that the splitting efficiency, depending on DQD energy level position ε and energy ω, takes values ranging from very low ($\eta \approx 0.2$) to its maximum value of $\eta = 1$. We recall that for $\eta = 1$ transport is exclusively due to CAR processes, while for $\eta = 0$, only DAR processes contribute to Andreev conductance; cf. Eq. (7). Clearly, large splitting efficiency is observed at low energies and for $-U - 2U_{LR} \lesssim \varepsilon \lesssim 0$; see Fig. 6(d). Moreover, a region of enhanced η is present in the Coulomb blockade regime with two electrons. Then, mainly CAR processes are responsible for Andreev transport. Note also that there are transport regimes where the splitting efficiency is rather poor and mainly DAR processes are responsible for transport; see the transport regime with odd number of electrons for elevated energies $|\omega|$ in Fig. 6(d).

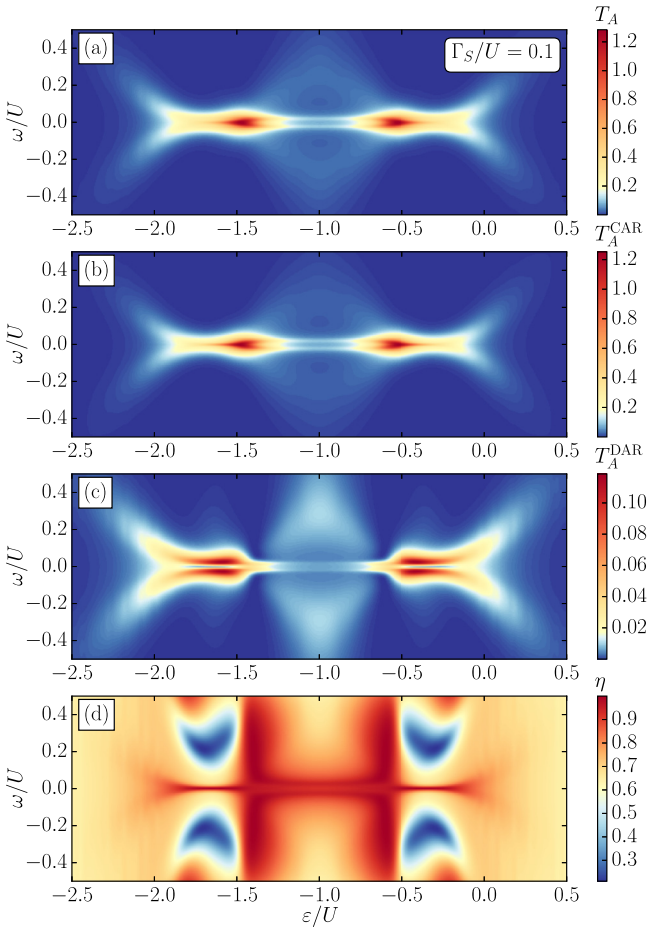

FIG. 6. (a) Total Andreev transmission coefficient and its contributions due to (b) CAR and (c) DAR processes, as well as (d) Cooper pair splitting efficiency η plotted as function of energy ω and double dot energy level position ε. The parameters are the same as in Fig. 3 with $\Gamma_S = U/10$.

The splitting efficiency greatly depends on the strength of coupling to superconductor. This dependence is explicitly demonstrated in Fig. 7, which shows the energy and DQD level dependence of η calculated for different values of Γ_S corresponding to those considered in Fig. 5. In this figure one can identify optimal parameters, for which the process of Cooper pair splitting is most efficient in the considered transport regime.

Finally, we would like to emphasize that the splitting efficiency also strongly depends on the ratio of interdot and intradot Coulomb correlations U/U_{LR}. In typical experimental realizations, $U \gg U_{LR}$, which is desired to enhance CAR processes and suppress DAR ones, obtaining thus large values of η. The splitting efficiency however generally decreases when the ratio of U/U_{LR} becomes smaller. In particular, the amount of DAR and CAR processes becomes equal when $U = U_{LR}$, such that $\eta = 1/2$ in the whole parameter space.

C. SU(2) Kondo regime

We now focus in greater detail on the SU(2) Kondo regime, where for $\Gamma_S = 0$ the DQD is occupied by two electrons, each on a different quantum dot; see Fig. 2. To simplify the

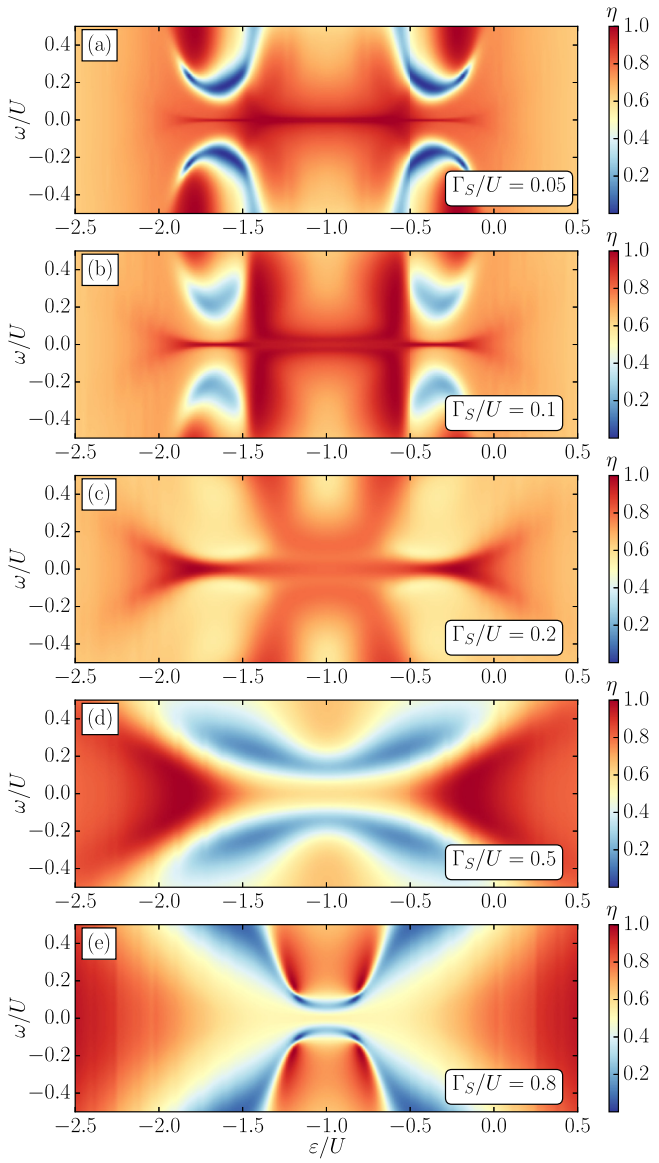

FIG. 7. Splitting efficiency η calculated for different values of coupling strength to superconducting lead, as indicated, and for parameters the same as in Fig. 3.

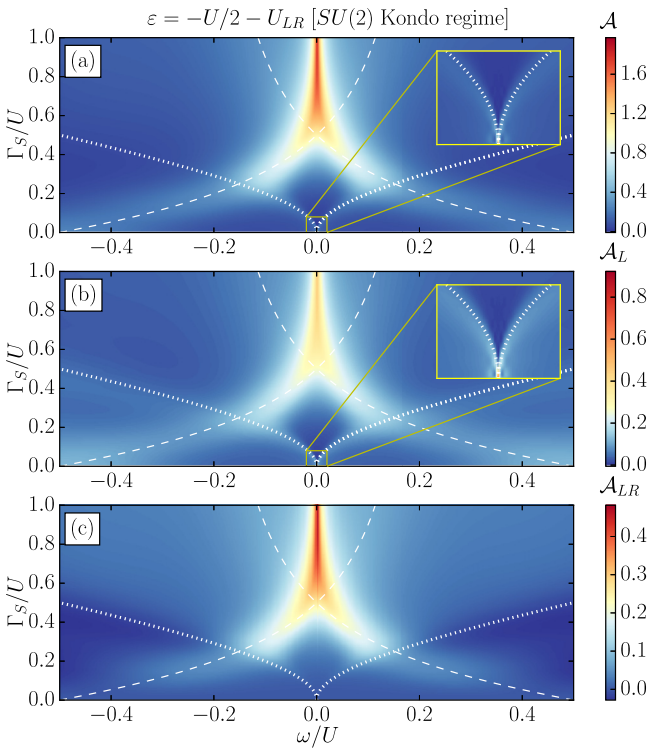

FIG. 8. Energy dependence of (a) the total normalized spectral function $\mathcal{A}$ and its contributions: (b) $\mathcal{A}_L$ and (c) $\mathcal{A}_{LR}$ calculated as a function of the coupling to superconductor Γ_S and for $\varepsilon = -U/2 - U_{LR}$. The insets show the zoom into the suppression of the SU(2) Kondo resonance with increasing Γ_S. The dashed lines indicate the energies of the Andreev bound states, cf. Eq. (12), while the dotted lines present the excitation energies between corresponding singlet and triplet states; cf. Eq. (13). The other parameters are as in Fig. 3.

discussion, we consider the particle-hole symmetry point of the model, $\varepsilon = -U/2 - U_{LR}$. Nevertheless, the conclusions drawn here shall apply to the whole two-electron Coulomb blockade regime where the spin SU(2) Kondo effect can develop.

The total normalized spectral function in the SU(2) Kondo regime, together with its contributions $\mathcal{A}_L$ and $\mathcal{A}_{LR}$, calculated as a function of Γ_S for $\varepsilon = -U/2 - U_{LR}$, is shown in Fig. 8. The dashed lines indicate the energies of the Andreev bound states, while the insets present the zooms into the low-energy behavior of the spectral function, where the suppression of the Kondo resonance with increasing Γ_S is clearly visible. The general behavior is as follows: finite coupling to superconductor results in the splitting and suppression of the Kondo resonance, which, however, emerges again for $\Gamma_S \approx U/2$. In fact, for this value of Γ_S, the system exhibits a phase transition and the ground state changes from spin singlet to spin doublet. Consequently, the Kondo resonance develops once $\Gamma_S \gtrsim U/2$; see Fig. 8.

Let us shed more light on the system's behavior by using some analytical arguments. For the particle-hole symmetry point, it is easy to find the eigenspectrum of the effective Hamiltonian (3). We will consider the lowest-energy singlet ($|S\rangle$), doublet ($|D_\sigma\rangle$), and triplet ($|T_\delta\rangle$) states. The first two states have the following explicit form:

$$|S\rangle = \alpha(|dd\rangle - |00\rangle) - \beta(|\uparrow\downarrow\rangle - |\downarrow\uparrow\rangle),$$
$$|D_\sigma\rangle = \tfrac{1}{2}(|\sigma 0\rangle + |0\sigma\rangle + |\sigma d\rangle + |d\sigma\rangle),$$

where the coefficients are given by $\alpha = \sqrt{(\gamma - U - U_{LR})/(4\gamma)}$, $\beta = 2\Gamma_S/\sqrt{\gamma(\gamma - U - U_{LR})}$, and $\gamma = \sqrt{(U + U_{LR})^2 + 16\Gamma_S^2}$. Note that these states correspond to the states $|D_\sigma^2\rangle$ and $|S_4\rangle$ presented in the Appendix. The triplet state is threefold degenerate with components $|T_+\rangle = |\uparrow\uparrow\rangle$, $|T_-\rangle = |\downarrow\downarrow\rangle$, and $|T_0\rangle = (|\uparrow\downarrow\rangle + |\downarrow\uparrow\rangle)/\sqrt{2}$. The energies of the above states are given by

$$E_S = -\tfrac{1}{2}\big[U + U_{LR} + \sqrt{(U + U_{LR})^2 + 16\Gamma_S^2}\big],$$
$$E_D = -\tfrac{1}{2}(U + 2U_{LR} + 4\Gamma_S),$$
$$E_T = -U - U_{LR}, \qquad (11)$$

respectively. Note that the energy of the triplet state does not depend on Γ_S. This is to be expected since the triplet state does not match the symmetry of the s-wave superconductor. The excitation energies between singlet and doublet states define the relevant ABS's energies

$$E_{ABS} = \pm\frac{U_{LR}}{2} \pm 2\Gamma_S \mp \frac{1}{2}\sqrt{(U+U_{LR})^2 + 16\Gamma_S^2}, \quad (12)$$

which are marked with dashed lines in Fig. 8.

In the case of $\Gamma_S = 0$, the singlet and triplet state are degenerate and the system exhibits the SU(2) Kondo effect on each quantum dot; see the insets in Figs. 8(a) and 8(b). However, when Γ_S becomes finite, the induced interdot pairing relevant for crossed Andreev reflection results in the singlet-triplet splitting and causes the singlet state $|S\rangle$ to be the ground state of the system. Because of that, the Kondo resonance gets very quickly suppressed when Γ_S increases and only split Kondo peaks are visible; see the insets in Fig. 8. The position of the split Kondo peaks is determined by the excitation energy between the singlet and triplet states, such that the peaks occur for

$$\omega \approx \pm\tfrac{1}{2}\big[U + U_{LR} - \sqrt{(U+U_{LR})^2 + 16\Gamma_S^2}\big]. \quad (13)$$

Thus, for small values of Γ_S, the position of side peaks depends in a parabolic way on the coupling to superconductor, $\omega \approx \pm 4\Gamma_S^2/(U+U_{LR})$. This parabolic dependence can be seen in Figs. 8(a) and 8(b) and the corresponding insets.

The value of Γ_S at which the Kondo resonance becomes suppressed can be estimated by comparing the characteristic energy scales, i.e., the Kondo temperature and the singlet-triplet excitation energy. One can then find the value of the coupling to superconductor, Γ_S^{TS}, at which the suppression of the Kondo resonance develops

$$\Gamma_S^{TS} \approx \tfrac{1}{2}\sqrt{T_{\rm K}^{SU(2)}(U+U_{LR})}. \quad (14)$$

For assumed parameters and recalling that $T_{\rm K}^{SU(2)}/U \approx 10^{-4}$, one gets $\Gamma_S^{TS}/U \approx 0.006$. This estimate is validated by NRG calculations of the total normalized spectral function for small values of Γ_S, which is plotted as a function of energy on logarithmic scale in Fig. 9(a). One can clearly see the Kondo peak for $\Gamma_S \ll \Gamma_S^{TS}$ and a gradual decrease of its height with increasing Γ_S, until the peak becomes completely suppressed for $\Gamma_S \gtrsim \Gamma_S^{TS}$. The vertical dashed lines in Fig. 9(a) mark the energy of the side Kondo peak as estimated from Eq. (13). The agreement between this analytical formula and full numerical calculations is quite satisfactory.

For $\Gamma_S \gtrsim \Gamma_S^{TS}$ and such values of Γ_S that the ground state is spin singlet, the system does not exhibit the Kondo effect at all. The spectral function reveals then just peaks at energies corresponding to the Andreev bound states; see Fig. 8. When, however, the energies of Andreev bound states cross the zero energy for $\Gamma_S \approx \Gamma_S^{SD}$, with

$$\Gamma_S^{SD} = \frac{U(U+2U_{LR})}{8U_{LR}} \quad (15)$$

(for assumed parameters this happens when $\Gamma_S^{SD} = U/2$), the doublet state $|D_\sigma\rangle$ becomes the ground state of the system. Then, one observes the reemergence of the Kondo resonance. This is explicitly presented in Fig. 9(b), which shows the total

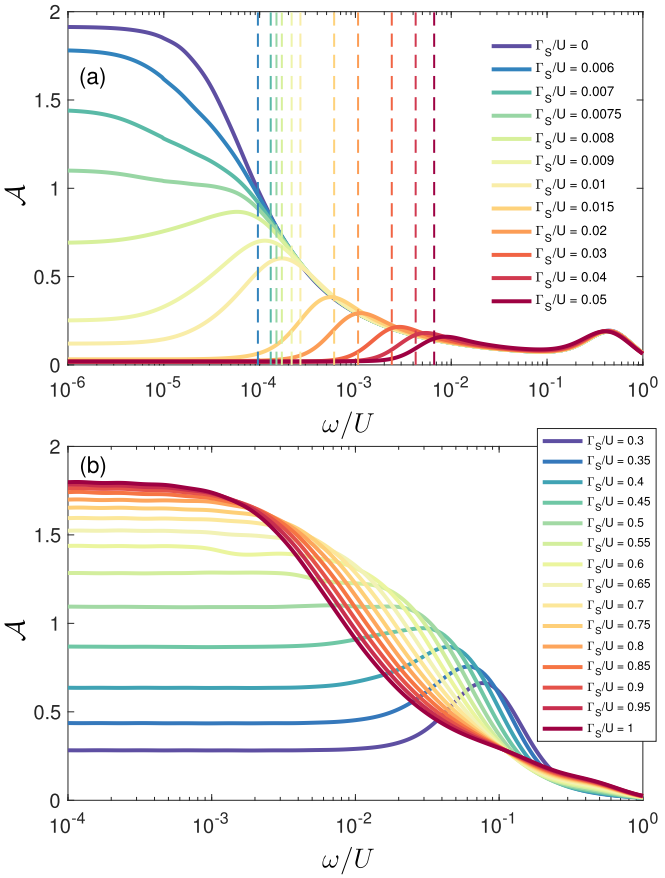

FIG. 9. Total normalized spectral function $\mathcal{A}$ plotted vs energy on logarithmic scale for selected values of Γ_S. Panel (a) presents the suppression of the Kondo resonance with Γ_S, which occurs for the critical value of $\Gamma_S = \Gamma_S^{TS} \approx 0.006U$; cf. Eq. (14). The vertical dashed lines in (a) show the excitation energies between the singlet and triplet states for given Γ_S; cf. Eq. (13). At these excitation energies side Kondo peaks occur. Panel (b) presents the restoration of the Kondo effect when $\Gamma_S \gtrsim \Gamma_S^{SD}$. The parameters are the same as in Fig. 8.

normalized spectral function plotted on logarithmic energy scale for the corresponding values of Γ_S. Note that the Kondo temperature is now clearly larger compared to the case of $\Gamma_S = 0$; cf. Figs. 9(a) and 9(b). This basically results from the difference in excitation energies to virtual states allowing for spin-flip processes driving the Kondo effect. For $\Gamma_S = 0$, the energy is given by the charging energy of each dot, while for $\Gamma_S \gtrsim \Gamma_S^{SD}$, it is given by the doublet-singlet excitation energy, which is smaller than U. Consequently, there is a larger exchange interaction in the latter case, which explains the observed difference in Kondo temperatures.

It is also interesting to notice that the maximum value of $\mathcal{A}$ at $\omega = 0$ is comparable for $\Gamma_S = 0$ and $\Gamma_S = U$, and approaches 2; see Fig. 9. In the former case this limit can be easily understood since each of the two quantum dots contributes with the Kondo resonance, such that $\mathcal{A}_L = \mathcal{A}_R \to 1$. In the latter case, on the other hand, one finds $\mathcal{A}_L = \mathcal{A}_R \to 1/2$ and $\mathcal{A}_{LR} = \mathcal{A}_{RL} \to 1/2$, cf. Fig. 8, which implies that the off-diagonal spectral function, that encompasses cross correlations between the two dots, contributes $1/(\pi\Gamma)$ to the height of the Kondo peak in the total spectral function.

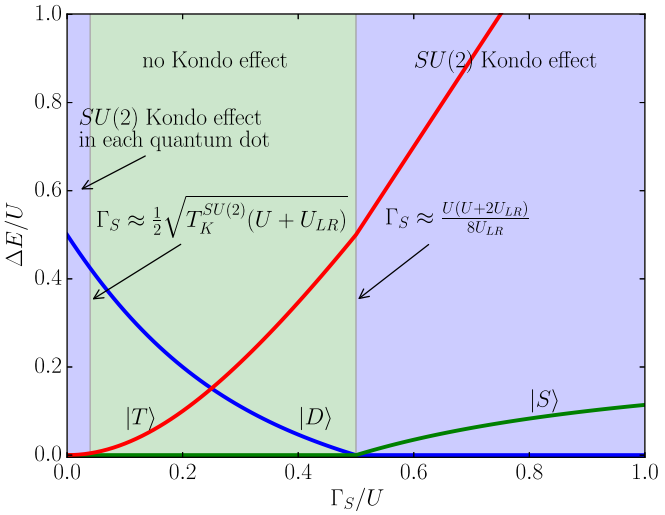

FIG. 10. Excitation energies ΔE between the singlet, doublet, and triplet states plotted as a function of the coupling to superconductor for parameters the same as in Fig. 8. The excitation energies are measured relative to the ground state energy, which is set to zero. The evolution of the ground state from the singlet ($|S\rangle$) to the doublet ($|D\rangle$) state is clearly visible. The values of Γ_S at which the Kondo effect becomes suppressed or emerges are indicated. $T_K^{SU(2)}$ denotes the SU(2) Kondo temperature for $\Gamma_S = 0$. Note that for $\Gamma_S = 0$ the singlet and triplet ($|T\rangle$) states are degenerate.

The low-energy behavior of the system in the two-electron transport regime is summarized in Fig. 10, which shows the evolution of the excitation energies ΔE between the relevant states, cf. Eq. (11), when Γ_S is varied. For two indicated values of Γ_S, the transport behavior of the system greatly changes. When $\Gamma_S \lesssim \Gamma_S^{TS}$, the Kondo singlet is the ground state of the system and the electrons experience a $\pi/2$ phase shift [29]. At $\Gamma_S \approx \Gamma_S^{TS}$, there is a crossover, such that for $\Gamma_S^{TS} \lesssim \Gamma_S \lesssim \Gamma_S^{SD}$, the interdot pairing-induced singlet becomes the ground state of the system. Consequently, there is no Kondo effect (phase shift is equal to zero). On the other hand, when $\Gamma_S \approx \Gamma_S^{SD}$, the system exhibits a phase transition and for $\Gamma_S \gtrsim \Gamma_S^{SD}$ the doublet state becomes the ground state of the splitter. This results in the reemergence of the Kondo effect.

Note that the system's behavior as a function of Γ_S is completely different from the case of a single quantum dot. In single quantum dots attached to superconducting and normal leads, in the subgap transport regime, the increase of Γ_S results in an enhancement of the Kondo temperature [43]. Since in the case of DQD for $\Gamma_S = 0$ the Kondo effect develops on each quantum dot, one could naively expect that for finite Γ_S the behavior will be qualitatively the same as in the single quantum dot case. The above-presented analysis clearly demonstrates that such conjecture is completely unjustified. The proximity-induced interdot pairing potential spoils this picture and, once $\Gamma_S \gtrsim \Gamma_S^{TS}$, it immediately results in the suppression of the Kondo resonance on both quantum dots. Thus the coupling to superconductor has a strong *destructive* influence on the SU(2) Kondo effect in DQD-based Cooper pair splitters. Note also that a very large value of the coupling Γ_S, i.e., $\Gamma_S \gtrsim \Gamma_S^{SD}$, can induce the Kondo effect again.

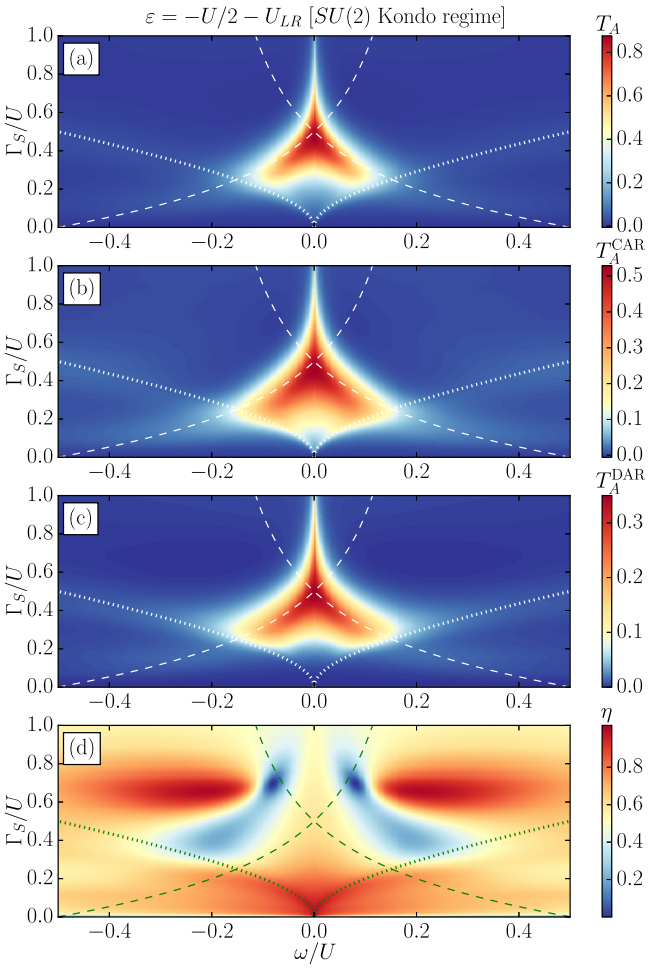

FIG. 11. (a) Total Andreev transmission coefficient and its contributions due to (b) CAR and (c) DAR processes, as well as (d) the Cooper pair splitting efficiency η plotted as function of energy ω and the strength of coupling to superconductor Γ_S. The dashed lines indicate the energies of the Andreev bound states given by Eq. (12), while the dotted lines present the excitation energies between corresponding singlet and triplet states given by Eq. (13). The parameters are the same as in Fig. 8.

Let us now analyze the behavior of the Andreev transmission, its contributions due to DAR and CAR processes, and the splitting efficiency in the SU(2) Kondo regime. The dependence of these quantities on energy and strength of coupling to superconductor is presented in Fig. 11. First of all, one can see that the transmission coefficient achieves considerable values mainly in the low-energy regime, in between the Andreev bound states. Moreover, an enhancement of transmission can be also seen along the energies of Andreev bound states; see Fig. 11. Interestingly, we note that for small values of Γ_S and low energies, mainly CAR processes dominate transport, which results in almost perfect splitting efficiency; see Fig. 11(d). We recall that this is the regime of suppressed and split Kondo resonance, which now we can clearly associate with the interdot pairing generated by crossed Andreev reflection. Note that despite suppression of the Kondo effect, in this transport regime $T_A^{\mathrm{CAR}}(\omega)$ is still considerable and extends to energy regions greater than $T_K^{SU(2)}$. When

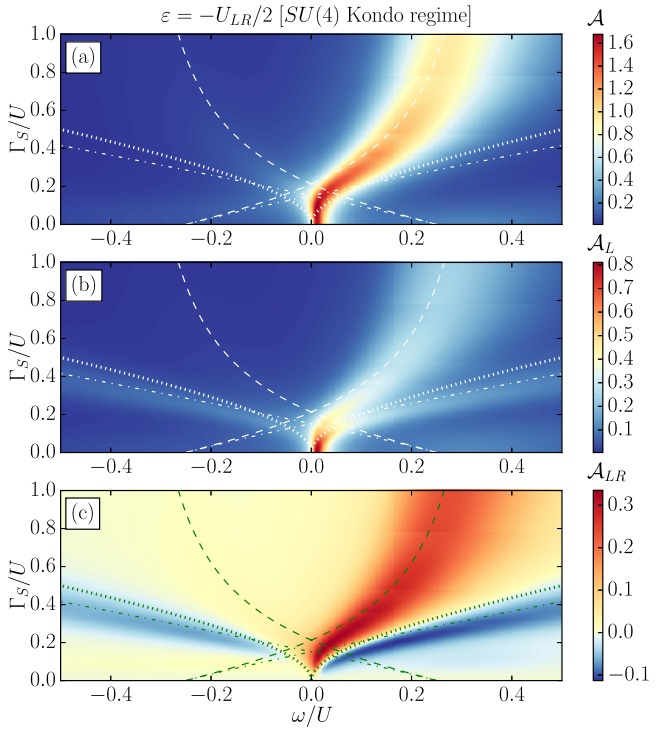

FIG. 12. Energy dependence of (a) the total normalized spectral function $\mathcal{A}$ and its contributions: (b) $\mathcal{A}_L$ and (c) $\mathcal{A}_{LR}$ calculated as a function of the coupling to superconductor Γ_S and for $\varepsilon = -U_{LR}/2$. The dashed and dotted-dashed lines indicate the energies of the Andreev bound states, while the dotted line shows the splitting of the doublet states, as given by Eq. (18). The other parameters are as in Fig. 3.

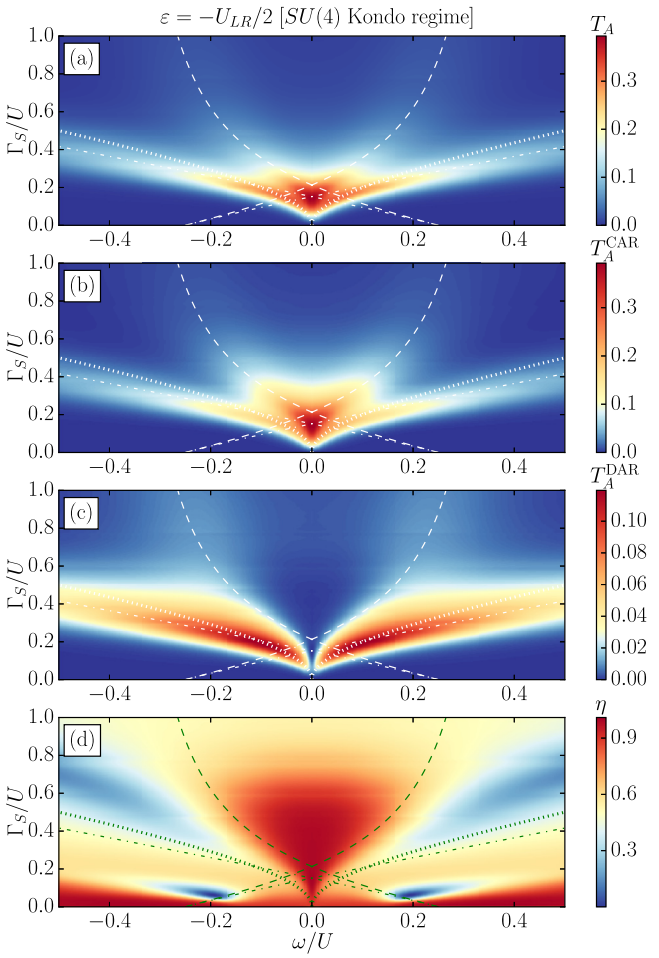

FIG. 13. (a) Total Andreev transmission coefficient and its contributions due to (b) CAR and (c) DAR processes, as well as (d) the Cooper pair splitting efficiency η plotted as function of energy ω and the strength of coupling to superconductor Γ_S for parameters the same as in Fig. 12. The dashed and dotted-dashed lines indicate the energies of the Andreev bound states, and the dotted line shows the splitting of the doublet states, as described by Eq. (18).

$\Gamma_S \gtrsim \Gamma_S^{SD}$, at low energies the splitting efficiency is smaller and it indicates that CAR and DAR processes contribute to Andreev transport on an equal footing. On the other hand, for larger energies, η first becomes suppressed and then increases again. However, in this transport regime the total transmission is relatively low; see Fig. 11.

D. SU(4) Kondo regime

In this section we consider more thoroughly the behavior of the spectral function and Andreev transmission in the SU(4) Kondo regime; see also Fig. 2. For $\Gamma_S = 0$ and when the DQD is singly occupied, the system exhibits the SU(4) Kondo effect resulting from the spin and orbital degeneracies. For the present analysis we thus assume $\varepsilon = -U_{LR}/2$. The normalized spectral function calculated as a function of energy and the strength of coupling to superconductor is shown in Fig. 12. At first sight, one can deduce that for relatively low values of Γ_S, i.e., $\Gamma_S \lesssim U/5$, the SU(4) Kondo resonance is hardly affected by the superconducting proximity effect. Only when the coupling to superconductor becomes larger ($\Gamma_S \gtrsim U/5$) does the Kondo phenomenon get suppressed—the resonance in the spectral function becomes then broadened and departs to larger energies. In fact, for $\Gamma_S \approx U/5$, the ground state of the system changes from the spin doublet to spin singlet state, and this is the reason for vanishing of the Kondo effect. For $\Gamma_S \gtrsim U/5$, $\mathcal{A}$ exhibits only resonances at larger energies corresponding to the Andreev bound state energies; see the dashed and dotted-dashed lines in Fig. 12, which mark the energies of Andreev bound states. The ABS's energies were determined from the excitation energies between appropriate singlet and doublet states obtained from numerical solution of the eigenvalue problem. The resonances associated with excitations due to Andreev bound states are also clearly visible in the spectral function of individual quantum dots $\mathcal{A}_L$ as well as in $\mathcal{A}_{LR}$, shown in Figs. 12(b) and 12(c), respectively.

At energies corresponding to Andreev bound states, the Andreev transmission coefficient also becomes enhanced. This can be seen in Fig. 13, which presents the energy ω and Γ_S dependence of $T_A(\omega)$ and its contributions due to CAR and DAR processes, together with the splitting efficiency η. We again notice that generally $T_A^{\mathrm{CAR}}(\omega) > T_A^{\mathrm{DAR}}(\omega)$ [cf. Figs. 13(b) and 13(c)], which leads to large splitting efficiency, especially visible for low energies [Fig. 13(d)]. In fact, for $\Gamma_S \approx U/5$, i.e., when the doublet-singlet transition occurs, the total transmission coefficient has a local maximum, which

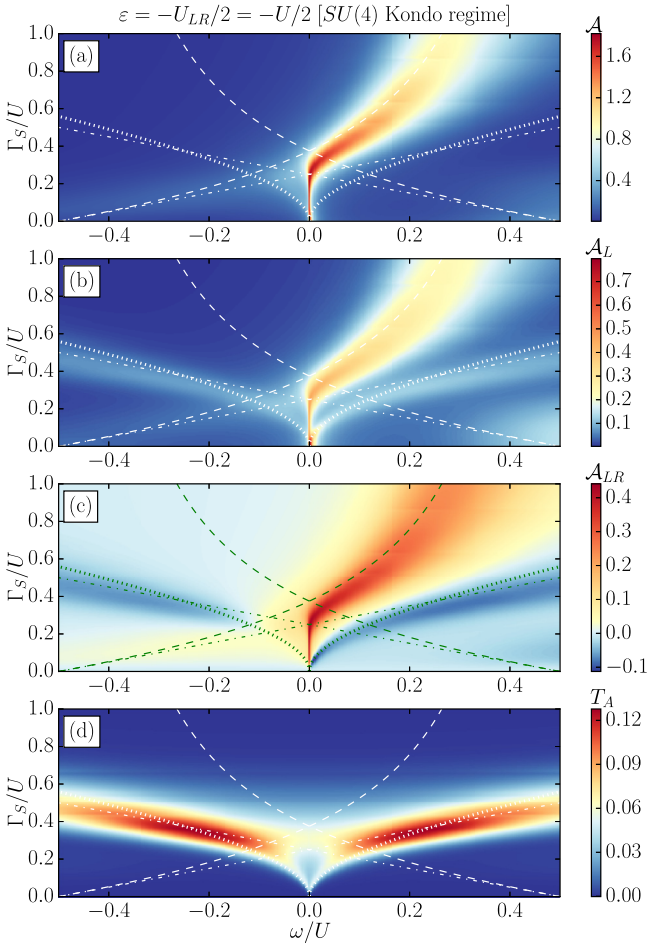

FIG. 14. Energy dependence of (a) the total normalized spectral function $\mathcal{A}$, its contributions (b) $\mathcal{A}_L$ and (c) $\mathcal{A}_{LR}$, and (d) the total Andreev transmission coefficient $T_A(\omega)$ plotted as a function of energy ω and Γ_S in the SU(4) Kondo regime for the symmetric case with $U_{LR} = U$. The dotted-dashed (dashed) lines indicate the energies of the Andreev bound states E^1_{ABS} (E^2_{ABS}), cf. Eq. (22), while the dotted lines show the doublet splitting energy; cf. Eq. (18). The other parameters are the same as in Fig. 3.

results mainly from CAR processes; see Fig. 13. Consequently, the splitting efficiency becomes then very close to unity. On the other hand, there are also transport regimes where η is very much suppressed, which indicates that DAR processes are dominant; see the transport region for $|\omega| \approx U/5$ and low values of Γ_S ($\Gamma_S \approx U/10$) in Fig. 13(d). The transmission coefficient in these transport regimes is however relatively low.

To shed more light on the influence of superconducting pairing correlations on the SU(4) Kondo regime, let us now assume a fully symmetric situation, namely $U_{LR} = U$. For this case, the dependence of the relevant spectral functions and the total Andreev transmission coefficient on ω and Γ_S is shown in Fig. 14. In the symmetric case, one can find the eigenenergies and eigenstates in the spin singlet subspace explicitly. These are presented in Table III in the Appendix, while the eigenspectrum in the doublet subspace can be found in Table I. Note that in the doublet subspace we can find the eigenspectrum for arbitrary parameters; therefore, if only

TABLE I. Eigenvalues and unnormalized eigenvectors of the effective DQD Hamiltonian in the doublet subspace. Here, $\Delta_D = [(2\varepsilon + 2U_{LR} + U)^2 + 16\Gamma_S^2]^{\frac{1}{2}}$ and $\alpha = (2\varepsilon + 2U_{LR} + U + \Delta_D)/(4\Gamma_S)$.

State	Eigenenergy	Eigenvector
$\lvert D^1_\sigma\rangle$	ε	$\lvert\sigma 0\rangle - \lvert 0\sigma\rangle$
$\lvert D^2_\sigma\rangle$	$2\varepsilon + U_{LR} + \frac{U-\Delta_D}{2}$	$\alpha(\lvert\sigma 0\rangle + \lvert 0\sigma\rangle) + \lvert\sigma d\rangle + \lvert d\sigma\rangle$
$\lvert D^3_\sigma\rangle$	$2\varepsilon + U_{LR} + \frac{U+\Delta_D}{2}$	$\lvert\sigma 0\rangle + \lvert 0\sigma\rangle - \alpha(\lvert\sigma d\rangle + \lvert d\sigma\rangle)$
$\lvert D^4_\sigma\rangle$	$3\varepsilon + 2U_{LR} + U$	$\lvert\sigma d\rangle - \lvert d\sigma\rangle$

the doublet states are considered we will present the analytical formulas for the general case of $U_{LR} \neq U$. From the inspection of the spectrum of H^{eff}_{DQD} one can see that for $\Gamma_S \to 0$ the ground state is indeed fourfold degenerate and given by the doublet states

$$\left|D^1_\sigma\right\rangle = \frac{1}{\sqrt{2}}(|\sigma 0\rangle - |0\sigma\rangle) \tag{16}$$

with energy $E^1_D = -U_{LR}/2$ and

$$\left|D^2_\sigma\right\rangle = \frac{1}{\sqrt{16\Gamma_S^2+\alpha^2}}[\alpha(|\sigma 0\rangle+|0\sigma\rangle) + 4\Gamma_S(|\sigma d\rangle+|d\sigma\rangle)], \tag{17}$$

with $\alpha = U + U_{LR} + \sqrt{(U+U_{LR})^2 + 16\Gamma_S^2}$, and the energy, $E^2_D = U/2 - \sqrt{(U+U_{LR})^2 + 16\Gamma_S^2}/2$. With increasing Γ_S, the two doublet states become split and the ground state is given by the state $|D^2_\sigma\rangle$. The doublet splitting energy is given by

$$\omega = \pm\tfrac{1}{2}\left[U + U_{LR} - \sqrt{(U+U_{LR})^2 + 16\Gamma_S^2}\right]. \tag{18}$$

This energy difference is marked with dotted lines in Figs. 12, 13, and 14. It coincides with the resonances in the spectral function $\mathcal{A}_L$ obtained from NRG calculations. These resonances are however not visible in the total spectral function, since the peak in $\mathcal{A}_L$ is counterbalanced by an associated minimum in $\mathcal{A}_{LR}$; see, e.g., Figs. 12(b) and 12(c). Pronounced maxima can be also observed in the Andreev transmission coefficient shown in Figs. 13 and 14(d). Note that while around the Fermi energy both the spectral function and Andreev transmission show features at the doublet-doublet excitation energy [Eq. (18)], for larger ω, the resonances occur at energies corresponding rather to the Andreev bound states.

The influence of the superconducting pairing correlations on the SU(4) Kondo state can be better resolved in the spectral function plotted versus energy on logarithmic scale. This is presented in Fig. 15. Now, one can clearly see that the maximum in the spectral function strongly depends on Γ_S. For very small pairing correlations, $\mathcal{A}$ exhibits a resonance at finite ω; see Fig. 15. Now for assumed parameters and $\Gamma_S = 0$ one finds $T_K^{SU(4)}/U \approx 0.004$. However, with increasing Γ_S, this resonance becomes suppressed and moves towards the Fermi energy. This is a clear indication of a crossover from the SU(4) to the SU(2) Kondo effect. Finite pairing correlations break the fourfold degeneracy of the ground state and reduce it to twofold degeneracy due to only the spin degrees of freedom. Because

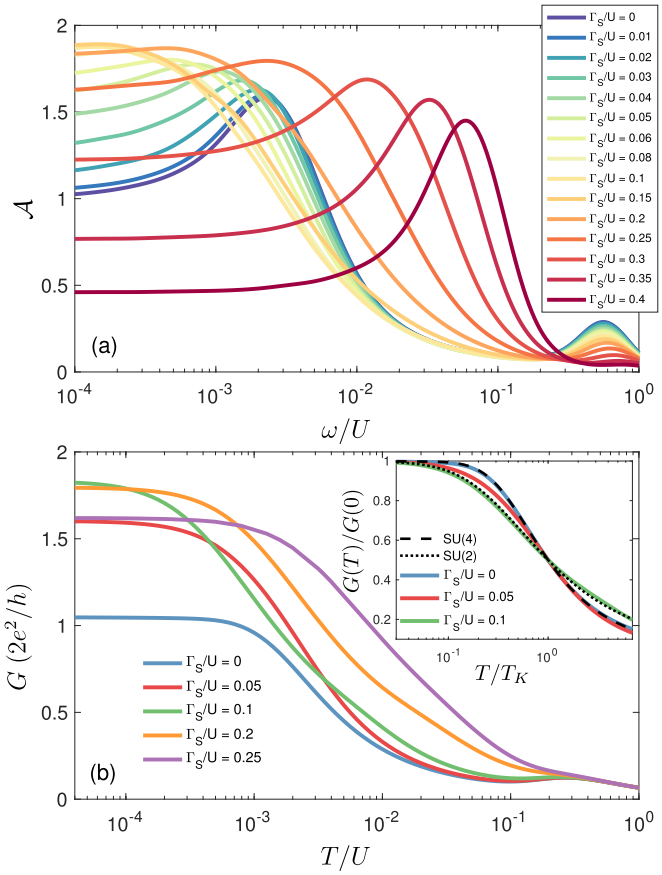

FIG. 15. (a) Total spectral function plotted vs energy on logarithmic scale and (b) the temperature dependence of the linear-response normal conductance for different values of Γ_S, as indicated in the legends. The inset in (b) presents the crossover of the universal scaling of the conductance vs T/T_K from the SU(4) to the SU(2) Kondo regime. The other parameters are the same as in Fig. 14. For $\Gamma_S = 0$ and assumed parameters $T_K^{SU(4)}/U \approx 0.004$.

of that, the SU(4) Kondo effect becomes suppressed. One can estimate the strength of coupling Γ_S when this crossover takes place (Γ_S^{DD}) by comparing the doublet splitting energy with the corresponding Kondo temperature. This leads to

$$\Gamma_S^{DD} \approx \tfrac{1}{2}\sqrt{T_K^{SU(4)}(U + U_{LR})}. \tag{19}$$

For parameters assumed in Fig. 15 one then finds $\Gamma_S^{DD} \approx 0.045U$. This estimate agrees reasonably well with the numerical data shown in Fig. 15(a).

Moreover, we corroborate the SU(4)-SU(2) crossover by calculating the temperature dependence of the normal conductance, which for potential drop between the left and right leads in the linear response regime can be expressed as [23,64]

$$G = \frac{2e^2}{h}\int d\omega\left(-\frac{\partial f(\omega)}{\partial\omega}\right)\mathcal{A}, \tag{20}$$

where $f(\omega)$ is the Fermi-Dirac distribution function. We note that, since the total conductance may contain contributions from Andreev reflection processes, the normal conductance G should be considered as a theoretical tool to gain information about the type of scaling and, thus, the type of the Kondo effect in the system. The temperature dependence of G is shown in Fig. 15(b). For $\Gamma_S = 0$, $G(T)$ exhibits the SU(4) universal scaling; see the inset in Fig. 15(b). However, with increasing Γ_S, e.g., for $\Gamma_S = 0.05U \gtrsim \Gamma_S^{DD}$, the scaling does not collapse onto the SU(4) universal function any more. Instead, for $\Gamma_S > \Gamma_S^{DD}$, one finds that the SU(2) Kondo effect becomes responsible for the conductance enhancement. The conductance reveals the SU(2) universal scaling for Γ_S up to $\Gamma_S \approx 3U/10$ (not shown), since for larger Γ_S the doublet is not the ground state of the system any more and the Kondo effect is not present in the system.

Note also that the maximum value of the low-temperature conductance, which corresponds directly to $\mathcal{A}$ at $\omega = 0$, depends in a nonmonotonic fashion on Γ_S. For $\Gamma_S = 0$, $G = 2e^2/h$, while for $\Gamma_S^{DD} \lesssim \Gamma_S$, G is clearly larger than $2e^2/h$ and approaches almost $4e^2/h$; see Fig. 15(b). This can be understood by realizing that finite coupling to a superconductor leads to an enhancement of the average occupation of each dot, such that the occupation of the double dot becomes larger than one. Moreover, finite coupling to a superconductor results in a large enhancement of $\mathcal{A}_{LR}$, such that the total conductance reaches $G \approx 4e^2/h$.

When the coupling to superconductor is enhanced further, a doublet-singlet transition occurs for $\Gamma_S = 3U/8$. For $\Gamma_S > 3U/8$, the ground state of the system is given by the following singlet state (cf. state $|S_2\rangle$ in Table III):

$$|S\rangle = \frac{1}{\sqrt{2}}\left[|00\rangle + \frac{1}{2}(|d0\rangle + |0d\rangle) + \frac{1}{2}(|\uparrow\downarrow\rangle - |\downarrow\uparrow\rangle)\right], \tag{21}$$

with the energy $E_S = -2\Gamma_S$. The excitations between the singlet and the two doublet states allow us to estimate the analytical formulas for the energies of the relevant Andreev bound states, which are given by

$$E_{ABS}^1 = \pm\frac{U}{2} \mp 2\Gamma_S,$$
$$E_{ABS}^2 = \pm\frac{U}{2} \pm 2\Gamma_S \mp \sqrt{U^2 + 4\Gamma_S^2}. \tag{22}$$

The energies of those Andreev bound states are presented in Fig. 14 with dotted-dashed and dashed lines, respectively. In fact, for $\Gamma_S > 3U/8$, the resonances present in the spectral function for positive energies are exactly due to the Andreev bound states; see Fig. 14. At the ABS energy E_{ABS}^1 an enhancement of the Andreev transmission is also clearly present; see Fig. 14(d).

Summing up, in the SU(4) Kondo regime, i.e., for $\varepsilon = -U/2$ with $U_{LR} = U$, the SU(4) Kondo effect is present for $\Gamma_S \lesssim \Gamma_S^{DD}$. At $\Gamma_S \approx \Gamma_S^{DD}$, there is an SU(4)-SU(2) crossover, and for $\Gamma_S^{DD} \lesssim \Gamma_S \lesssim 3U/8$ the system exhibits the SU(2) Kondo resonance. When $\Gamma_S \approx 3U/8$, there is a phase transition and the ground state changes from the spin doublet to the spin singlet state, such that for larger values of Γ_S the system does not exhibit the Kondo effect any more. These findings are schematically summarized in Fig. 16, which shows the evolution of the ground state when the strength of coupling to superconductor increases.

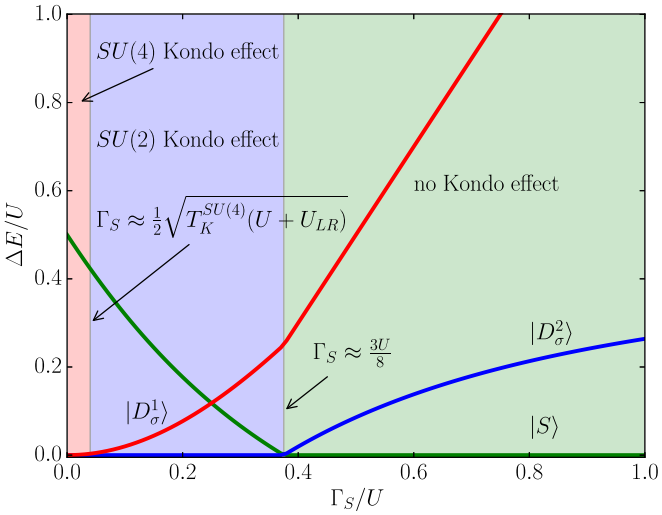

FIG. 16. Excitation energies ΔE between the corresponding singlet and two doublet states plotted as a function of the coupling to superconductor for parameters the same as in Fig. 14. The excitation energies are measured relative to the ground state energy, which is set to zero. The values of Γ_S at which the symmetry of the Kondo state or the ground state of the system changes are indicated.

IV. CONCLUSIONS

We have analyzed the transport properties of double quantum dot based Cooper pair splitters strongly coupled to external electrodes, focusing on the Kondo regime. The two dots were attached to a common s-wave superconductor and each dot was coupled to a separate metallic electrode. The considerations were performed in the subgap transport regime, where transport was driven by direct and crossed Andreev reflection processes. By using the density-matrix numerical renormalization group method, we determined the behavior of the local density of states of DQD and the Andreev transmission coefficient, together with Cooper-pair splitting efficiency. First, we have analyzed the dependence of the transport properties on the position of the DQD energy levels and then we have focused on the SU(2) and SU(4) Kondo regimes.

We have shown that the superconducting pairing correlations can greatly influence the Kondo effect in the system. In the SU(2) Kondo regime, we predict a very quick suppression of the Kondo resonance with increasing the strength of coupling to superconductor. This effect is in stark contrast to the single quantum dot case, where increase of pairing correlations resulted in an enhancement of the Kondo temperature [43,47]. The disappearance of the SU(2) Kondo peak is directly associated with the formation of a spin singlet state between the two quantum dots triggered by proximity-induced interdot pairing potential. With increasing the strength of coupling to superconductor further, we demonstrate that the system undergoes a transition to the doublet state. In this transport regime, the Kondo effect reemerges and the total spectral function shows a pronounced Kondo peak. The occurrence of this resonance is associated with contributions coming from both individual quantum dots $\mathcal{A}_i$, as well as from cross correlations described by the off-diagonal part of the spectral function $\mathcal{A}_{ij}$.

In the SU(4) Kondo regime, on the other hand, the impact of superconducting pairing correlations on the Kondo state is less abrupt and now the Kondo effect persists for larger couplings to superconductor as compared to the SU(2) case. More specifically, we predict that, in the fully symmetric situation, the SU(4) Kondo effect becomes first reduced to the SU(2) Kondo effect, which becomes then fully suppressed once $\Gamma_S > 3U/8$. For this value of coupling to superconductor, the ground state changes from the spin doublet to the proximity-induced singlet state and, consequently, there is no Kondo effect. The spectral function exhibits then only resonances at energies corresponding to energies of Andreev bound states. Interestingly, in the SU(4) Kondo regime, when $U_{LR} < U$, we find that the Andreev current is mainly due to CAR processes, which yields almost perfect Cooper pair splitting efficiency.

Finally, we would like to note that most of our findings, and especially the suppression or reemergence of the Kondo state as the coupling to superconductor is varied, could be tested with the present-day experimental technology. We hope that our research will stimulate further efforts in this direction.

ACKNOWLEDGMENTS

We acknowledge discussions with Kacper Bocian. This work was supported by the National Science Centre in Poland through the Project No. DEC-2013/10/E/ST3/00213. Computing time at Poznań Supercomputing and Networking Center is acknowledged.

APPENDIX: SPECTRUM OF THE EFFECTIVE DOUBLE DOT HAMILTONIAN

Here we present the eigenvalues and eigenvectors of isolated double quantum dot with proximity-induced pairing potentials, as modeled by the effective Hamiltonian (3). Because the Hamiltonian possesses the full spin SU(2) symmetry, we can write $H_{DQD}^{\rm eff}$ in blocks labeled by the spin quantum number. Moreover, it is enough to use 10 spin multiplets instead of 16 local states. Let us first start from the trivial triplet subspace. The triplet state $|T_\delta\rangle$ has the components: $|T_+\rangle = |\uparrow\uparrow\rangle$, $|T_-\rangle = |\downarrow\downarrow\rangle$, $|T_0\rangle = (|\uparrow\downarrow\rangle + |\downarrow\uparrow\rangle)/\sqrt{2}$, and the energy $E_T = 2\varepsilon + U_{LR}$.

The Hamiltonian block in the spin doublet subspace is explicitly given by

$$H_{DQD}^{\rm eff,S=\frac{1}{2}} = \begin{pmatrix} \varepsilon & 0 & -\Gamma_S & -\Gamma_S \\ 0 & \varepsilon & -\Gamma_S & -\Gamma_S \\ -\Gamma_S & -\Gamma_S & \varepsilon_3 & 0 \\ -\Gamma_S & -\Gamma_S & 0 & \varepsilon_3 \end{pmatrix}, \tag{A1}$$

with $\varepsilon_3 = 3\varepsilon + 2U_{LR} + U$. This matrix is written in the following states: $|\sigma 0\rangle$, $|0\sigma\rangle$, $|\sigma d\rangle$, and $|d\sigma\rangle$, respectively, and its eigenvalues together with unnormalized eigenvectors are listed in Table I.

Now, let us consider the singlet subspace which is spanned by the following five states: $|00\rangle$, $|d0\rangle$, $|0d\rangle$, $|S_0\rangle = (|\uparrow\downarrow\rangle - |\downarrow\uparrow\rangle)/\sqrt{2}$, and $|dd\rangle$. The effective DQD Hamiltonian in this

TABLE II. Eigenvalues and unnormalized eigenvectors of the effective DQD Hamiltonian in the singlet subspace for the particle-hole symmetry point, $\varepsilon = -U/2 - U_{LR}$. Here, $\Delta_S = (U_{LR}^2 + 4\Gamma_S^2)^{\frac{1}{2}}$, $\alpha = (U_{LR} + \Delta_S)/(2\Gamma_S)$, and $\tilde{\Delta}_S = [(U + U_{LR})^2 + 16\Gamma_S^2]^{\frac{1}{2}}$.

State	Eigenenergy	Eigenvector
$\|S_1\rangle$	$-2U_{LR}$	$\|d0\rangle - \|0d\rangle$
$\|S_2\rangle$	$-U_{LR} - \Delta_S$	$\|dd\rangle + \|00\rangle + \alpha(\|d0\rangle + \|0d\rangle)$
$\|S_3\rangle$	$-U_{LR} + \Delta_S$	$\alpha(\|dd\rangle + \|00\rangle) - \|d0\rangle - \|0d\rangle$
$\|S_4\rangle$	$-\frac{U+U_{LR}+\tilde{\Delta}_S}{2}$	$\|dd\rangle - \|00\rangle + \frac{U+U_{LR}+\tilde{\Delta}_S}{2\sqrt{2}\Gamma_S}\|S_0\rangle$
$\|S_5\rangle$	$-\frac{U+U_{LR}-\tilde{\Delta}_S}{2}$	$\|dd\rangle - \|00\rangle + \frac{U+U_{LR}-\tilde{\Delta}_S}{2\sqrt{2}\Gamma_S}\|S_0\rangle$

subspace is given by

$$H_{DQD}^{\text{eff,S=0}} = \begin{pmatrix} 0 & -\Gamma_S & -\Gamma_S & \sqrt{2}\Gamma_S & 0 \\ -\Gamma_S & 2\varepsilon + U & 0 & 0 & -\Gamma_S \\ -\Gamma_S & 0 & 2\varepsilon + U & 0 & -\Gamma_S \\ \sqrt{2}\Gamma_S & 0 & 0 & 2\varepsilon + U_{LR} & -\sqrt{2}\Gamma_S \\ 0 & -\Gamma_S & -\Gamma_S & -\sqrt{2}\Gamma_S & \varepsilon_4 \end{pmatrix}, \tag{A2}$$

TABLE III. Eigenvalues and unnormalized eigenvectors of the effective DQD Hamiltonian in the singlet subspace in the SU(4) Kondo regime, that is for $\varepsilon = -U/2$ and $U_{LR} = U$. Here, $\Delta_S = (U^2 + \Gamma_S^2)^{\frac{1}{2}}$ and $\alpha = (U + \Delta_S)/(2\Gamma_S)$.

State	Eigenenergy	Eigenvector
$\|S_1\rangle$	0	$\|d0\rangle - \|0d\rangle$
$\|S_2\rangle$	$-2\Gamma_S$	$\|S_0\rangle - \sqrt{2}\|00\rangle - \frac{1}{\sqrt{2}}(\|d0\rangle + \|0d\rangle)$
$\|S_3\rangle$	$2\Gamma_S$	$\|S_0\rangle + \sqrt{2}\|00\rangle - \frac{1}{\sqrt{2}}(\|d0\rangle + \|0d\rangle)$
$\|S_4\rangle$	$2U - 2\Delta_S$	$\alpha(\|d0\rangle + \|0d\rangle + \sqrt{2}\|S_0\rangle) + \|dd\rangle$
$\|S_5\rangle$	$2U + 2\Delta_S$	$\alpha\|dd\rangle - (\|d0\rangle + \|0d\rangle + \sqrt{2}\|S_0\rangle)$

where $\varepsilon_4 = 4\varepsilon + 2U + 4U_{LR}$ is the energy of the fully occupied double dot. The first eigenstate is $|S_1\rangle = (|d0\rangle - |0d\rangle)/\sqrt{2}$ and its eigenenergy reads $2\varepsilon + U$. The next eigenenergies are given by polynomials of various Hamiltonian parameters and do not have simple analytical structure; therefore, we will not present them here. Instead, let us consider some limiting situations. The first one is relevant to the SU(2) Kondo regime, $\varepsilon = -U/2 - U_{LR}$, and the second one is associated with the SU(4) Kondo regime, when $\varepsilon = -U_{LR}/2$ and $U = U_{LR}$. The eigenspectrum in the former case is presented in Table II, while the states and energies in the latter case are listed in Table III.

[1] D. Loss and D. P. DiVincenzo, Quantum computation with quantum dots, Phys. Rev. A **57**, 120 (1998).

[2] B. Ruggiero, P. Delsing, C. Granata, Y. A. Pashkin, and P. Silvestrini, *Quantum Computing in Solid State Systems* (Springer-Verlag, New York, 2006).

[3] M. A. Nielsen and I. L. Chuang, *Quantum Computation and Quantum Information: 10th Anniversary Edition* (Cambridge University Press, Cambridge, UK, 2011).

[4] P. Recher, E. V. Sukhorukov, and D. Loss, Andreev tunneling, Coulomb blockade, and resonant transport of nonlocal spin-entangled electrons, Phys. Rev. B **63**, 165314 (2001).

[5] M. Tinkham, *Introduction to Superconductivity: Second Edition (Dover Books on Physics) (Vol. I)* (Dover Publications, Mineola, NY, 2004).

[6] D. Ciudad, Superconductivity: Splitting Cooper pairs, Nat. Mater. **14**, 463 (2015).

[7] L. Hofstetter, S. Csonka, J. Nygård, and C. Schönenberger, Cooper pair splitter realized in a two-quantum-dot y-junction, Nature (London) **461**, 960 (2009).

[8] L. G. Herrmann, F. Portier, P. Roche, A. L. Yeyati, T. Kontos, and C. Strunk, Carbon Nanotubes as Cooper-Pair Beam Splitters, Phys. Rev. Lett. **104**, 026801 (2010).

[9] L. Hofstetter, S. Csonka, A. Baumgartner, G. Fülöp, S. d'Hollosy, J. Nygård, and C. Schönenberger, Finite-Bias Cooper Pair Splitting, Phys. Rev. Lett. **107**, 136801 (2011).

[10] J. Schindele, A. Baumgartner, and C. Schönenberger, Near-Unity Cooper Pair Splitting Efficiency, Phys. Rev. Lett. **109**, 157002 (2012).

[11] A. Das, Y. Ronen, M. Heiblum, D. Mahalu, A. V. Kretinin, and H. Shtrikman, High-efficiency Cooper pair splitting demonstrated by two-particle conductance resonance and positive noise cross-correlation, Nat. Commun. **3**, 1165 (2012).

[12] G. Fülöp, S. d'Hollosy, A. Baumgartner, P. Makk, V. A. Guzenko, M. H. Madsen, J. Nygård, C. Schönenberger, and S. Csonka, Local electrical tuning of the nonlocal signals in a Cooper pair splitter, Phys. Rev. B **90**, 235412 (2014).

[13] G. Fülöp, F. Domínguez, S. d'Hollosy, A. Baumgartner, P. Makk, M. H. Madsen, V. A. Guzenko, J. Nygård, C. Schönenberger, A. Levy Yeyati, and S. Csonka, Magnetic Field Tuning and Quantum Interference in a Cooper Pair Splitter, Phys. Rev. Lett. **115**, 227003 (2015).

[14] Z. B. Tan, D. Cox, T. Nieminen, P. Lähteenmäki, D. Golubev, G. B. Lesovik, and P. J. Hakonen, Cooper Pair Splitting by Means of Graphene Quantum Dots, Phys. Rev. Lett. **114**, 096602 (2015).

[15] A. F. Andreev, The Thermal conductivity of the intermediate state of superconductors, Zh. Eksp. Teor. Fiz. **46**, 1823 (1964) [Sov. Phys. JETP **19**, 1228 (1964)].

[16] D. Beckmann, H. B. Weber, and H. v. Löhneysen, Evidence for Crossed Andreev Reflection in Superconductor-Ferromagnet Hybrid Structures, Phys. Rev. Lett. **93**, 197003 (2004).

[17] J. Gramich, A. Baumgartner, and C. Schönenberger, Resonant and Inelastic Andreev Tunneling Observed on a Carbon Nanotube Quantum Dot, Phys. Rev. Lett. **115**, 216801 (2015).

[18] D. Sherman, J. S. Yodh, S. M. Albrecht, J. Nygård, P. Krogstrup, and C. M. Marcus, Normal, superconducting and topological

regimes of hybrid double quantum dots, Nat. Nanotechnol. **12**, 212 (2017).
[19] Y. Tanaka, N. Kawakami, and A. Oguri, Correlated electron transport through double quantum dots coupled to normal and superconducting leads, Phys. Rev. B **81**, 075404 (2010).
[20] J. Eldridge, M. G. Pala, M. Governale, and J. König, Superconducting proximity effect in interacting double-dot systems, Phys. Rev. B **82**, 184507 (2010).
[21] D. Chevallier, J. Rech, T. Jonckheere, and T. Martin, Current and noise correlations in a double-dot Cooper-pair beam splitter, Phys. Rev. B **83**, 125421 (2011).
[22] J. Barański and T. Domański, Decoherence effect on fano line shapes in double quantum dots coupled between normal and superconducting leads, Phys. Rev. B **85**, 205451 (2012).
[23] P. Trocha and J. Barnaś, Spin-polarized Andreev transport influenced by Coulomb repulsion through a two-quantum-dot system, Phys. Rev. B **89**, 245418 (2014).
[24] B. Sothmann, S. Weiss, M. Governale, and J. König, Unconventional superconductivity in double quantum dots, Phys. Rev. B **90**, 220501 (2014).
[25] P. Trocha and I. Weymann, Spin-resolved Andreev transport through double-quantum-dot Cooper pair splitters, Phys. Rev. B **91**, 235424 (2015).
[26] R. Hussein, L. Jaurigue, M. Governale, and A. Braggio, Double quantum dot Cooper-pair splitter at finite couplings, Phys. Rev. B **94**, 235134 (2016).
[27] K. Wrześniewski, P. Trocha, and I. Weymann, Current cross-correlations in double quantum dot based Cooper pair splitters with ferromagnetic leads, J. Phys.: Condens. Matter **29**, 195302 (2017).
[28] J. Kondo, Resistance minimum in dilute magnetic alloys, Prog. Theor. Phys. **32**, 37 (1964).
[29] A. C. Hewson, *The Kondo Problem to Heavy Fermions* (Cambridge University Press, Cambridge, UK, 1997).
[30] D. Goldhaber-Gordon, H. Shtrikman, D. Mahalu, D. Abusch-Magder, U. Meirav, and M. A. Kastner, The Kondo effect in a single-electron transistor, Nature (London) **391**, 156 (1998).
[31] S. M. Cronenwett, T. H. Oosterkamp, and L. P. Kouwenhoven, A tunable Kondo effect in quantum dots, Science **281**, 540 (1998).
[32] L. Borda, G. Zaránd, W. Hofstetter, B. I. Halperin, and J. von Delft, SU(4) Fermi Liquid State and Spin Filtering in a Double Quantum Dot System, Phys. Rev. Lett. **90**, 026602 (2003).
[33] A. J. Keller, S. Amasha, I. Weymann, C. P. Moca, I. G. Rau, J. A. Katine, H. Shtrikman, G. Zaránd, and D. Goldhaber-Gordon, Emergent SU(4) Kondo physics in a spin-charge-entangled double quantum dot, Nat. Phys. **10**, 145 (2014).
[34] S. De Franceschi, L. Kouwenhoven, C. Schonenberger, and W. Wernsdorfer, Hybrid superconductor-quantum dot devices, Nat. Nanotechnol. **5**, 703 (2010).
[35] A. Martin-Rodero and A. Levy Yeyati, Josephson and Andreev transport through quantum dots, Adv. Phys. **60**, 899 (2011).
[36] E. J. H. Lee, X. Jiang, R. Aguado, G. Katsaros, C. M. Lieber, and S. De Franceschi, Zero-Bias Anomaly in a Nanowire Quantum Dot Coupled to Superconductors, Phys. Rev. Lett. **109**, 186802 (2012).
[37] J.-D. Pillet, P. Joyez, R. Žitko, and M. F. Goffman, Tunneling spectroscopy of a single quantum dot coupled to a superconductor: From Kondo ridge to Andreev bound states, Phys. Rev. B **88**, 045101 (2013).
[38] E. J. H. Lee, X. Jiang, M. Houzet, R. Aguado, C. M. Lieber, and S. De Franceschi, Spin-resolved Andreev levels and parity crossings in hybrid superconductor-semiconductor nanostructures, Nat. Nanotechnol. **9**, 79 (2014).
[39] J. Bauer, A. Oguri, and A. C. Hewson, Spectral properties of locally correlated electrons in a Bardeen-Cooper-Schrieffer superconductor, J. Phys.: Condens. Matter **19**, 486211 (2007).
[40] R. Maurand and C. Schönenberger, Viewpoint: To screen or not to screen, that is the question! Physics **6**, 75 (2013).
[41] K. J. Franke, G. Schulze, and J. I. Pascual, Competition of superconducting phenomena and Kondo screening at the nanoscale, Science **332**, 940 (2011).
[42] B.-K. Kim, Y.-H. Ahn, J.-J. Kim, M.-S. Choi, M.-H. Bae, K. Kang, J. S. Lim, R. López, and N. Kim, Transport Measurement of Andreev Bound States in a Kondo-Correlated Quantum Dot, Phys. Rev. Lett. **110**, 076803 (2013).
[43] T. Domański, I. Weymann, M. Barańska, and G. Górski, Constructive influence of the induced electron pairing on the Kondo state, Sci. Rep. **6**, 23336 (2016).
[44] K. G. Wilson, The renormalization group: Critical phenomena and the Kondo problem, Rev. Mod. Phys. **47**, 773 (1975).
[45] Ö. Legeza, C. P. Moca, A. I. Tóth, I. Weymann, and G. Zaránd, Manual for the flexible DM-NRG code, arXiv:0809.3143v1 (the open access Budapest code is available at http://www.phy.bme.hu/~dmnrg/).
[46] R. Bulla, T. A. Costi, and T. Pruschke, Numerical renormalization group method for quantum impurity systems, Rev. Mod. Phys. **80**, 395 (2008).
[47] R. Žitko, J. S. Lim, R. López, and R. Aguado, Shiba states and zero-bias anomalies in the hybrid normal-superconductor Anderson model, Phys. Rev. B **91**, 045441 (2015).
[48] A. V. Rozhkov and D. P. Arovas, Interacting-impurity Josephson junction: Variational wave functions and slave-boson mean-field theory, Phys. Rev. B **62**, 6687 (2000).
[49] T. Yoichi, K. Norio, and O. Akira, Numerical renormalization group approach to a quantum dot coupled to normal and superconducting leads, J. Phys. Soc. Jpn. **76**, 074701 (2007).
[50] T. Meng, S. Florens, and P. Simon, Self-consistent description of Andreev bound states in Josephson quantum dot devices, Phys. Rev. B **79**, 224521 (2009).
[51] D. Futterer, M. Governale, M. G. Pala, and J. König, Nonlocal Andreev transport through an interacting quantum dot, Phys. Rev. B **79**, 054505 (2009).
[52] B. Sothmann, D. Futterer, M. Governale, and J. König, Probing the exchange field of a quantum-dot spin valve by a superconducting lead, Phys. Rev. B **82**, 094514 (2010).
[53] J. Barański and T. Domański, Fano-type interference in quantum dots coupled between metallic and superconducting leads, Phys. Rev. B **84**, 195424 (2011).
[54] D. Futterer, J. Swiebodzinski, M. Governale, and J. König, Renormalization effects in interacting quantum dots coupled to superconducting leads, Phys. Rev. B **87**, 014509 (2013).
[55] K. P. Wójcik and I. Weymann, Proximity effect on spin-dependent conductance and thermopower of correlated quantum dots, Phys. Rev. B **89**, 165303 (2014).
[56] I. Weymann and P. Trocha, Superconducting proximity effect and zero-bias anomaly in transport through quantum dots weakly attached to ferromagnetic leads, Phys. Rev. B **89**, 115305 (2014).

[57] I. Weymann and K. P. Wójcik, Andreev transport in a correlated ferromagnet-quantum-dot-superconductor device, Phys. Rev. B **92**, 245307 (2015).

[58] R. Chirla and C. P. Moca, Fingerprints of Majorana fermions in spin-resolved subgap spectroscopy, Phys. Rev. B **94**, 045405 (2016).

[59] S. Głodzik, K. P. Wójcik, I. Weymann, and T. Domański, Interplay between electron pairing and Dicke effect in triple quantum dot structures, Phys. Rev. B **95**, 125419 (2017).

[60] B. W. Heinrich, L. Braun, J. I. Pascual, and K. J. Franke, Protection of excited spin states by a superconducting energy gap, Nat. Phys. **9**, 765 (2013).

[61] A. Freyn and S. Florens, Optimal broadening of finite energy spectra in the numerical renormalization group: Application to dissipative dynamics in two-level systems, Phys. Rev. B **79**, 121102 (2009).

[62] W. C. Oliveira and L. N. Oliveira, Generalized numerical renormalization-group method to calculate the thermodynamical properties of impurities in metals, Phys. Rev. B **49**, 11986 (1994).

[63] W. G. van der Wiel, S. De Franceschi, J. M. Elzerman, T. Fujisawa, S. Tarucha, and L. P. Kouwenhoven, Electron transport through double quantum dots, Rev. Mod. Phys. **75**, 1 (2002).

[64] K. Bocian and W. Rudziński, Photon-assisted tunneling in a hybrid junction based on a quantum dot coupled to two ferromagnets and a superconductor, Phys. Status Solidi B **254**, 1600206 (2017).